Feasibility Study On The Use Of Navy Ranges For Basic Research In Underwater Acoustics

Final Report
U.S. Department of Defense
Office of Naval Research
800 North Quincy Street
Arlington, VA 22217-5660

Contract No: N00014-97-C-0174
CLIN/ACRN No: 0001/AA

SSI Report No: 970820-F012

Scientific Solutions, Inc.
18 Clinton Drive
Hollis, NH 03049-6576

Feasibility study on the use of Navy ranges for basic research in underwater acoustics

Subramaniam D. Rajan and Peter J. Stein
Scientific Solutions, Inc.
18 Clinton Drive , Hollis, NH 03049

1. Introduction

The Navy operates underwater tracking ranges which are used for system evaluation and training exercises. These ranges consist primarily of bottom mounted sources and receivers which are cabled to shore. The Navy also maintains support facilities at these installations which include data acquisition and processing systems. The sources and receivers deployed in these ranges are similar to those used for basic scientific research in underwater acoustics. These assets, which are available both in the Atlantic and Pacific, can therefore be utilized by the scientific community for basic research when they are not in use by the Navy. This dual-use of Navy assets will provide an inexpensive means of conducting meaningful year round basic scientific research.

More specifically, this report investigates the feasibility of using the Pacific Missile Range Facility (PMRF) located off Kauai, Hawaii, for conducting scientific research in underwater acoustics. PMRF was chosen for this study because it has by far the most extensive suite of underwater hardware. It is also undergoing expansion with a number of additional sources and receivers deployed in shallow water areas. The facilities at PMRF go well beyond the basic requirement for underwater tracking ranges. In-air RF based tracking and communications capabilities are extensive. Other facilities available at the PMRF site are support ships, shore facilities, and an airport.

The environment in the region of PMRF has special characteristics that make it an excellent choice for conducting acoustic propagation experiments. The depth of the water column falls off rapidly with range, providing a strong range dependent environment. This facility, therefore, affords an excellent opportunity for conducting long range acoustic propagation studies from a region extending from very shallow water to deep water. Further, since the facility is permanent, the time variability of the acoustic propagation characteristics can be studied. The tidal flow around the Hawaiian Islands gives rise to oceanographic features such as deep internal tides. Since the acoustic propagation is affected by the environment, the investigation of the oceanographic features is also important. The acoustic data can therefore be used to obtain images of the temperature field by performing tomography experiments.

2. Pacific Missile Range Facility

The location and layout of the PMRF tracking range is shown in Figure 1. It consists of two parts: a deep water region called BSURE (Barking Sands Underwater Range Expansion) and a region with shallower water depths called BARSTUR (Barking Sands Tactical Underwater Range). The BSURE part of the range covers over 880 square miles and the depth of water in this region is over 2200 m. There are a total of 18 bottom mounted receivers and 2 bottom mounted sources in this region. BARSTUR covers an area of 120 square miles and the depth of water ranges from 600 m to 2000 m. There are a total of 42 bottom mounted receivers and 3 bottom mounted sources in this area. An extension to this range known as SWTR (Shallow Water Training Range), which covers the shallow water areas of the ocean, is in progress and will be completed by October 1997. This extension covers an area of 82 square miles and its location is shown in Figure 2. The depth of water in this area ranges from 40 m to 600 m. A total of 118 bottom mounted receivers and 10 sources are to be deployed in this area. Therefore, including this new addition, the facility covers an area of about 1100 square miles with 16 sources and 178 receivers distributed over this area. The densest population of the receivers is in the shallow water area.

The locations of the sources and receivers with reference to $22^{0}07'10"N$ and $159^{0}55'10.2"W$ for the BARSTUR range are shown in Figure 3. The locations including the depths of the all the receivers and sources in BARSTUR are given in Tables 1 and 2 of Appendix A.

The sources in BSURE and BARSTUR operate at 8 -12 kHz. In the shallow water range SWTR two sources have an operating frequency of 1-3 kHz while the others work in the range of 8-12 kHz. The receivers have a wide bandwidth and are capable of receiving from 50 Hz to 20 kHz.

In the acquisition systems for the BSURE and BARSTUR ranges, the analog signal from the receivers are sent to the shore facility where they go through a patch panel to a FM recorder and tracking system. The system installed in the SWTR is digital. The signal is digitized at the receiver and transmitted via a fiber optic cable to shore where it is de-multiplexed and passed through a patch panel to D/A and then on to a recorder and tracking system.

3. Environment

3.1 Bottom bathymetry

The bathymetry of the region covered by PMRF ranges varies from 40 m in the shallowest area to over 4500m in the deep areas. Between the BARSTUR and BSURE areas, the bottom drops off steeply with the change from 600 m to 4500 m occurring over a range of approximately 65 km. A bathymetric chart of the region is shown in Figure 4.

3.2 Ocean bottom character

Figure 5 is the sidescan sonar image of the bottom in the region surrounding the island of Kauai. This was obtained using the Gloria system. The bottom in these deep water areas surrounding the island are characterized by regions of high reflectivity. This is due to the presence of rocky features such as outcroppings located either on the surface or buried under a layer of sediment. Figure 6 shows the bottom characteristics around the Hawaiian Islands obtained using subbottom profilers. The region close to the island is characterized by strong reflectors (Region colored green in Figure 6) as seen in the inset for subbottom profiling of this region.

3.3 Sound velocity profile

The average sound speed profile for the different seasons are shown in Figure 7. This averaged profile is based on the profiles obtained from CTD/XBT casts conducted in the area over long periods of time. We note that the seasonal changes in the sound speed profile are small. All profiles have a mixed layer of approximately 50 m followed by a strong thermocline with the lowest value of the sound speed occurring at a depth of approximately 700 m.

3.4 Oceanographic features

Regional waters around islands are commonly dominated by wind-driven and tidal flows. Among the tidal flows, one that is of particular interest is the deep internal tide which has been observed to occur in Mamla Bay, Hawaii. Figure 8 shows temperature variations on several moorings at a depth of 250 m in Mamla Bay, south of the Hawaiian Island of Oahu. Temperature variations at 250 m were commonly of the order of 3-4^{0}C and sometimes as large as 6-7^{0}C during the semi-diurnal tide. The oceanography of Kauai, including tidal action and geography, is very similar to Oahu and one would expect similar deep internal tides in this region as well.

The generation and propagation of internal tides, which occur about 200 m below the main pycnocline, is not well understood. Satellite altimetry indicates that internal tides propagate 300-1000 km from the Hawaiian ridge, but this has not yet been corroborated with temperature and acoustic data.

These deep tides, apart from its importance as an oceanographic feature that is not yet well understood, has strong operational implications, as they can impact weapon and acoustic sensor performance.

4. Acoustic Propagation

4.1 Propagation in a strongly range dependent environment

As we have noted in an earlier section, the PMRF site is characterized by a strong bathymetric variation. In this section we look at the propagation of sound in this range dependent environment. For the purpose of simulation we will assume that the range dependence arises only out of the bathymetric variations. The bottom characteristics

will be assumed to be range independent. The sound speed profile representing the mean of the four seasons (Figure 7) will be used as the profile for the water column. This profile has been extrapolated to include depths up to 4500m by assuming that the increase in sound speed with depth is only due to pressure and therefore has a gradient of 0.016 m/s/m. The bottom will be assumed to be a fluid with a compressional wave speed of 2000 m/s and a density of 2.0 gm/cc representing a strong reflector. The bathymetry is assumed to vary linearly from 600 m to 4500 m over a range of 65 km.

We now consider acoustic propagation from shallow depth to deep water. This corresponds to propagation from BARSTUR range to BSURE. In Figures 9 and 10 we show the contour plot of the transmission loss for a 2D slice with the propagation occurring out to a range of 65 km. The propagation loss was computed using the PE code MMPE. The two figures correspond to source depths of 300 m and 500 m respectively. The source frequency in both cases was 1 kHz. The simulations could not be performed at higher frequencies because of the limitations of the code. However, the results obtained at 1 kHz will provide information on the essential characteristics of the range dependent propagation. From the figures we note the following:

1. Propagation is strongly dependent on the source location.
2. For the two source locations, propagation into regions close to the ocean surface is not efficient beyond a range of approximately 10 km. This is because the rays turn around before reaching this region.
3. Penetration of energy into the sediment is strongest in regions close to the source in both cases.
4. For both source locations, the propagation in the mid-column region is efficient out to 65 km.
5. The transmission loss for regions close to the ocean floor reaches a value of 90 dB at a range of approximately 40 km. Since the receivers in the PMRF range are located on the ocean floor we are interested in determining whether these receiver locations are suitable for propagation studies. We note that when the source is placed close to the bottom we have efficient propagation to the receivers on the ocean floor up to a range of 40 km. Beyond that range, the acoustic field at the ocean floor falls off rapidly. This is because the sound speed profile which is upward refracting in the lower part of the sound speed profile prevents rays reaching deep parts of the ocean beyond 40 km in range.

Figures 11 and 12 show the contour plot of transmission loss for propagation from deep to shallow water simulating propagation from BSURE to BARSTUR. The two figures correspond to source depth of 2200 m and 3500 m respectively. In this case of up slope propagation, the transmission loss of 90 dB at the ocean bottom occurs at a range of 30 km for the deep source and 55 km for the source at mid-column. We therefore conclude that propagation out to ranges of 30 km can be studied with the sources and receivers placed close to the bottom.

4.2 Propagation through deep internal tide

One of the oceanographic features which is specific to this area is the formation of deep internal tides. Observations made off Oahu indicate the presence of strong internal

tides below the main pycnocline. These strong internal tides are of interest to the Navy as they can affect sensor performance.

Figure 13 shows the sound speed profile which indicates the presence of a strong temperature gradient below the main pycnocline occurring at a depth of 50 m. This profile was obtained based on the observations in the Mamla Bay, Hawaii. The sound speed profile in this case extends to a depth of only 500 m as the internal tides are generated in the shallow part of the ocean. The figure also shows the excursion of the sound speed profile (shown dotted in Figure 13) that occurs due to internal tides. We now examine the effect of the change in the sound speed profile on acoustic propagation. In this case the ocean is assumed to be of constant depth. The bottom properties were assumed to be the same as in the earlier case. Figures 14 to 17 show the contour plot of transmission loss for the two profiles in Figure 13. Figures 14 and 15 are for a source depth of 250 m and 16 and 17 are for a source depth of 450 m. We note from Figures 14 and 15 that when the source is at 250 m, (i.e. at the depth where the excursions in sound speed due to internal tides take place), the transmission loss is significantly affected by the presence of the tides. Figure 14 also shows the presence of a shadow zone. However, this feature is absent when the source is at the bottom. In this case, we note that the downward refracting profile in this region causes energy to be trapped close to the bottom and efficient propagation occurs in the region close to the ocean bottom all the way out to 30 km.

Considerable changes in acoustic propagation therefore occur due to presence of deep internal tides depending on the position of the source. It is therefore necessary to investigate the formation and propagation of deep internal tides which can be done by performing an acoustic tomography experiment. It is mentioned that a tomography experiment by a French consortium to study deep internal tides in the Bay of Biscay (INTIMATE98) is planned for 1998.

5. Model - Data Comparison

During December 1996, a small data set was collected using the PMRF facilities. A short, 9 kHz sineburst was transmitted from one of the sources in BARSTUR area (approximate water depth of 1700 m), and data were recorded at several hydrophones. Since we are proposing to use the bottom mounted sources and receivers, the arrival structure for this configuration of receivers needed to be explored, and this was the primary object of the simple experiment conducted.

During this experiment, XBT data were collected to determine the sound velocity profile in the area. The XBT measured the temperature structure up to a depth of 755 m. In Figure 18 we plot the sound velocity profile obtained from the XBT data and the average profile from historical data. We note that the profile from XBT data closely follows the profile from historical data. We therefore used the profile from the historical data to extend the profile from the XBT data up to a depth of 1750 m.

The data acquired during the experiment suffered from two important shortcomings. These were:

1. Only one short ping was transmitted. Therefore, no improvement to signal to noise ratio could be achieved by averaging over a number of pings. This restricted the range at which we could see arrivals to 5 km or less.
2. Data were collected for about 11 seconds after transmission of the signal. Therefore, receivers at ranges greater than 12 km did not show any arrivals.

Figure 19 shows the eigen rays for a source depth of 1700 m and a receiver depth of 1550 m. The range between source and receiver was 5 km. The figure shows only those rays which have not more than two interactions with the bottom. The arrival structure for these arrivals is shown in Figure 20.

To compare the arrival structure with field data, we examine the data acquired at hydrophone 4-6 which is at 5 km from the source (UQC 1). The source and receiver (hydrophone 4-6) depths are 1702 m and 1552 m, respectively. The scheme for acquiring the data was improvised since only existing facilities at PMRF were used. A short burst of a sine wave was sent from source UQC1. The arrival of this signal at hydrophone 4-8 triggered the acquisition of the signal by another hydrophone 4-6. From this the arrival time at hydrophone 4-6 with reference to the transmit time is determined. The raw signal acquired during the experiment at receiver 4-8 and 4-6 are shown in Figures 21 and 22. The arrival structure obtained from this data are also plotted in Figure 20. We note that early arrival which correspond to direct path is not seen in the data. However the arrival structure contains rays which have undergone interactions with the bottom. The absence of early arrival at this range may be due to the range dependent nature of the environment, both in the water column and the bottom bathymetry which were not incorporated in the model used. It is however felt that considerable enhancement in SNR can be achieved by using a long coded sequence and with such a signal it will be possible to identify arrivals at receivers well over 10 km.

The eigen rays for a receiver at a range of 30 km from the source is shown in Figure 23. We note that there are a number of rays which have less than two interactions with the bottom and will, therefore, provide stable paths for tomography experiments.

6. Acoustic Tomography Experiment

One of the issues that we considered was the feasibility of conducting an acoustic tomography experiment using the assets of the PMRF site. As we have noted earlier, an interesting oceanographic feature in the area is the deep internal tide. The primary purpose of this experiment will be to investigate the generation and propagation of deep internal tides. Since internal tides form in the shallow regions surrounding the island and propagate out to the deep waters, the sources and receivers in the BARSTUR and SWTR ranges can be used to study the formation of the tides. The propagation of the tides can be studied using the sources and receivers in the BSURE range.

In classical ocean acoustic tomography, the sources and receivers are on a vertical array and ray arrival times are used for estimating the sound speed structure in the regions between the sources and receivers. If only the earliest arrivals are used, the ray paths for short ranges are almost horizontal. This results in poor resolution in the horizontal. In order to improve the resolution in the horizontal, rays which interact with the boundaries and those which turn around in the water column will need to be included in the inversion. The ability to resolve features in the sound speed structure will then depend on the number of rays passing through a given region. When the ray density is large, we can expect good resolution. In regions where there are no rays, the resolution will be poor.

In the PMRF, both the sources and receivers are on the ocean floor. The ray diagram for this configuration is shown in Figure 24. The receivers form a horizontal array placed on the ocean floor. We note from the ray diagram, that except for a region close to the source, the rays sample the entire water column. We can therefore expect good resolution of the estimates. However, our ability to do this will depend on the attainable time resolution which is a function of the bandwidth of the signal. The smallest difference between successive arrivals is approximately 4.3 msec. Therefore a signal bandwidth of 500 Hz will be adequate to resolve the arrivals. This can be easily achieved.

We now present the results of a simple simulation study conducted to investigate the possibility of using bottom mounted sources and receivers in an ocean acoustic tomography experiment. We consider a situation where the sound speed in the water column is a function of depth only. We consider the two profiles in Figure 13. One of these is taken as the starting profile, (i.e. the profile at the commencement of the experiment). This is considered known by direct measurement. The second profile in Figure 13 is the target profile (i.e. we want to determine this profile from travel time data obtained from a field experiment after the sound speed profile has evolved into the target profile due to the presence of internal tides). The source is placed at a depth of 450 m and the receiver at a depth of 470 m in a water depth of 500 m. In Figures 25 and 26 we plot the ray diagram for the two profiles. For the starting profile there are 22 eigen rays in the figure. In the case of the target profile we have 14 eigen rays. We use the travel time data for these 14 rays and reconstruct the target profile. Since the starting profile gives rise to 22 rays, the rays which correspond to those in the case of the target profile were identified using travel time data. The reconstructed profile after three iterations is shown in Figure 27, together with the target and starting profiles. We note that the reconstruction is converging to the correct solution. We therefore conclude that bottom mounted sources and receivers can be successfully used to map the sound speed field in the region. The resolution of the estimates can be improved by the use of multiple sources and receivers.

7. Recommendations

In light of what has been described in the earlier paragraphs, it is considered that the facilities at the PMRF range can be effectively used to conduct basic research in underwater acoustics. **These ranges provide a unique opportunity for conducting**

long term acoustic experiments covering a three dimensional space. An added advantage is that the experiments can be performed at relatively low cost.

Before a large scale experiment is attempted, we recommend that the following work be undertaken which is considered a necessary precursor to any major field experiment.

7.1 Simulation of environmental conditions

Detailed bathymetric maps of the region exist. The water column properties are to be determined using existing hydrographic observations. The goal will be to produce a realistic T-S water column structure with appropriate spatial variations of the deep internal tides and other oceanographic features.

7.2 Simulation of acoustic propagation

The simulated environmental field, together with bathymetry data, are to be used to model the acoustic field in three dimensions. The goal will be to study the effect of changes in the bathymetry and oceanographic features on the propagation of the acoustic field in shallow and deep water areas using existing 3D models. The results of the simulation study will be validated in an experiment by measuring the field at all the receivers distributed on the ocean floor.

7.3 Numerical study of acoustic tomography experiment

A numerical acoustic tomography experiment is to be performed to investigate the feasibility of using the existing PMRF assets. As the source frequency is in the region of 8 to 10 kHz, transmission over long ranges will be difficult to achieve. However, since there are a number of sources, a subset of the sources can be used to obtain the temperature field in a number of overlapping regions which can then be integrated to obtain the image for the entire region. The results of the numerical experiment are to be used to assess the feasibility of this approach. The numerical simulations can also be used to determine the optimal experimental configuration for the tomography experiment.

7.4 Preliminary acoustic propagation and tomography experiment.

Based on the results of the simulation studies, an experiment is to be designed with limited goals. This will be a precursor to a major experiment to be undertaken at a later date. The goals are:

a) To determine the improvement in SNR attainable with the use of long coded sequences.
b) To develop a system that can transmit a coded signal from the bottom mounted sources.
c) To develop a data acquisition system that can be integrated with existing PMRF facilities and record data at a number of hydrophones.
d) To perform a preliminary tomography and propagation experiment to study the structure of deep internal tides and three dimensional propagation.

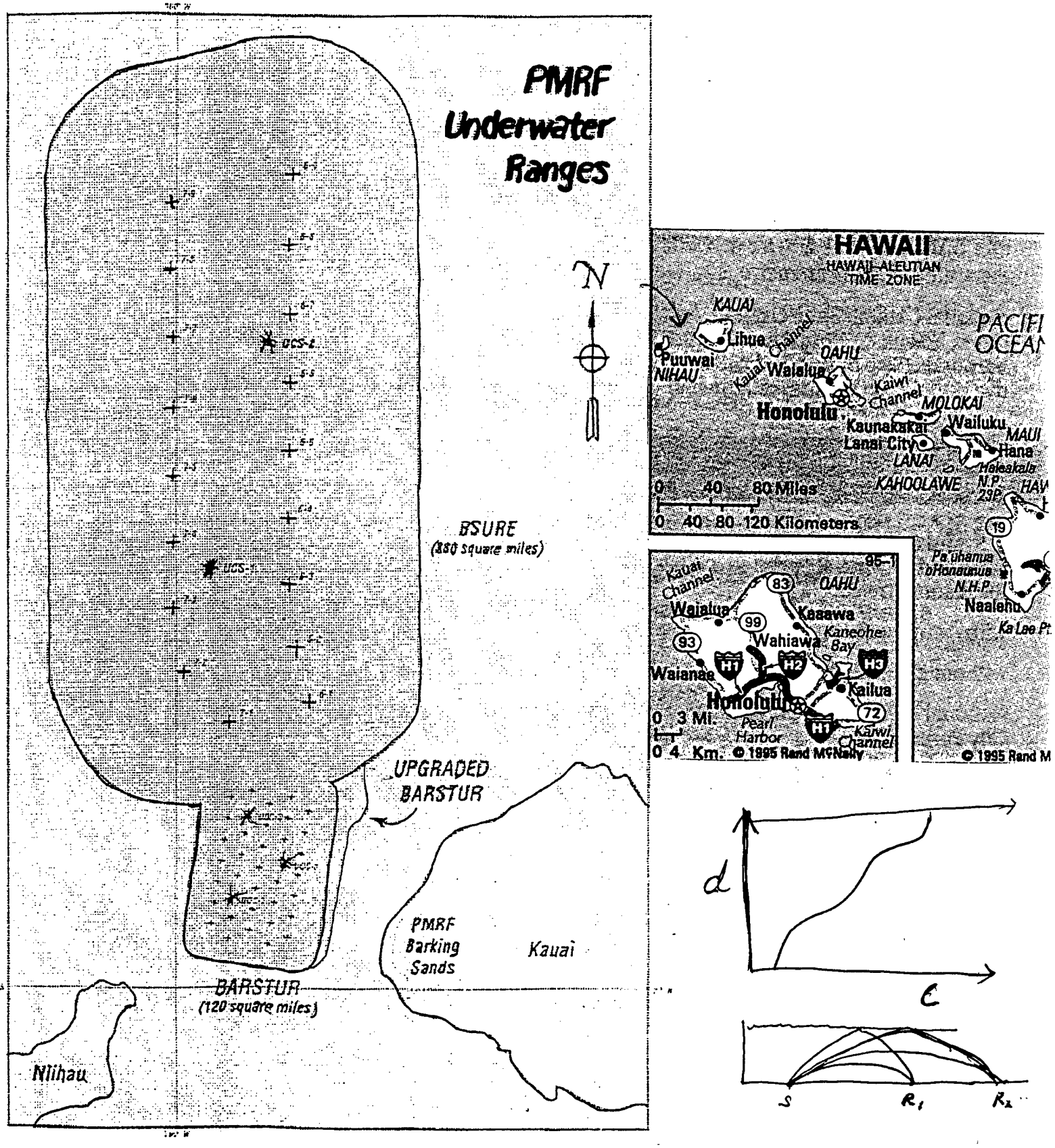

Figure 1. BSURE and BARSTUR ranges at PMRF.

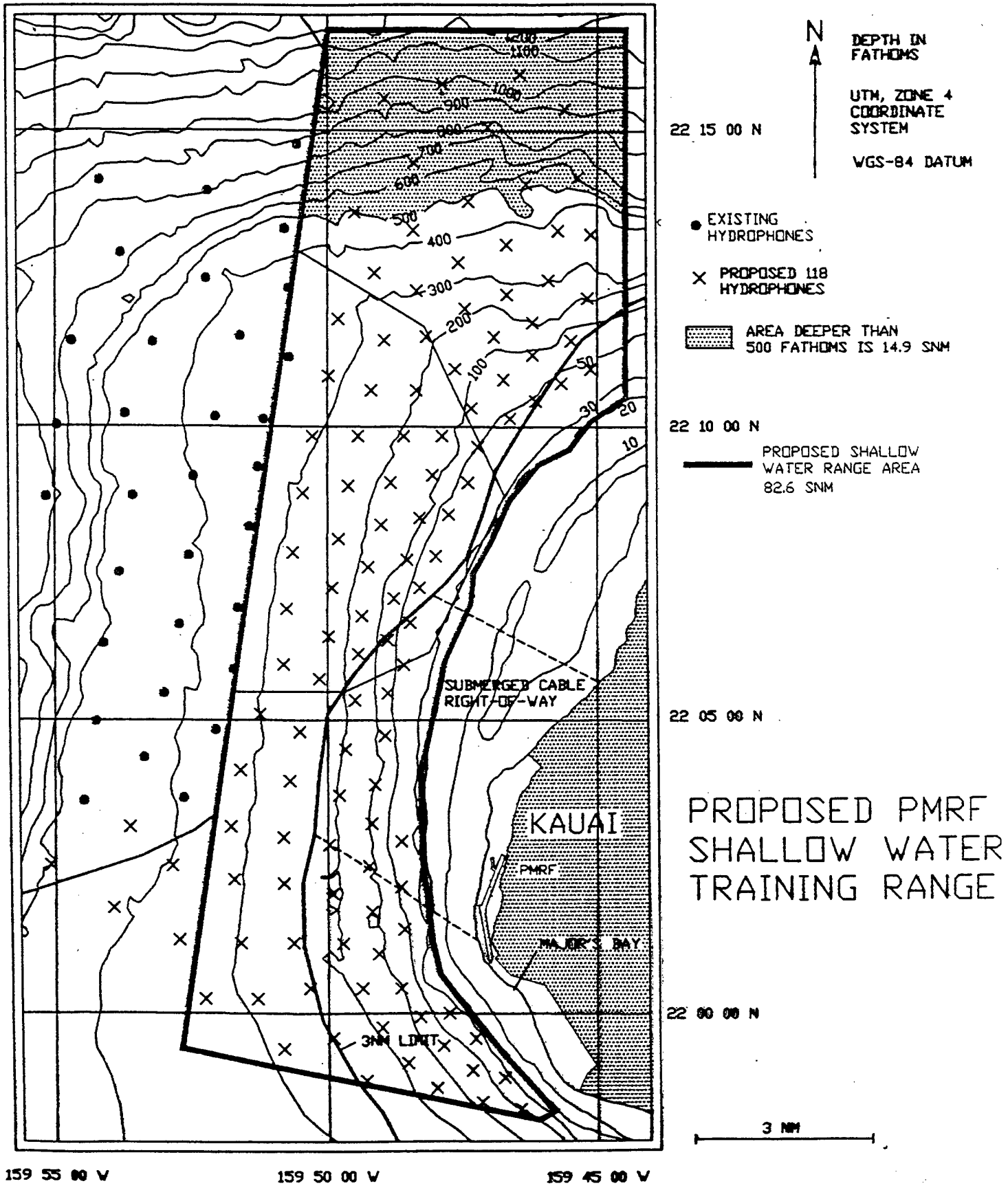

Figure 2. Extension to PMRF under construction.

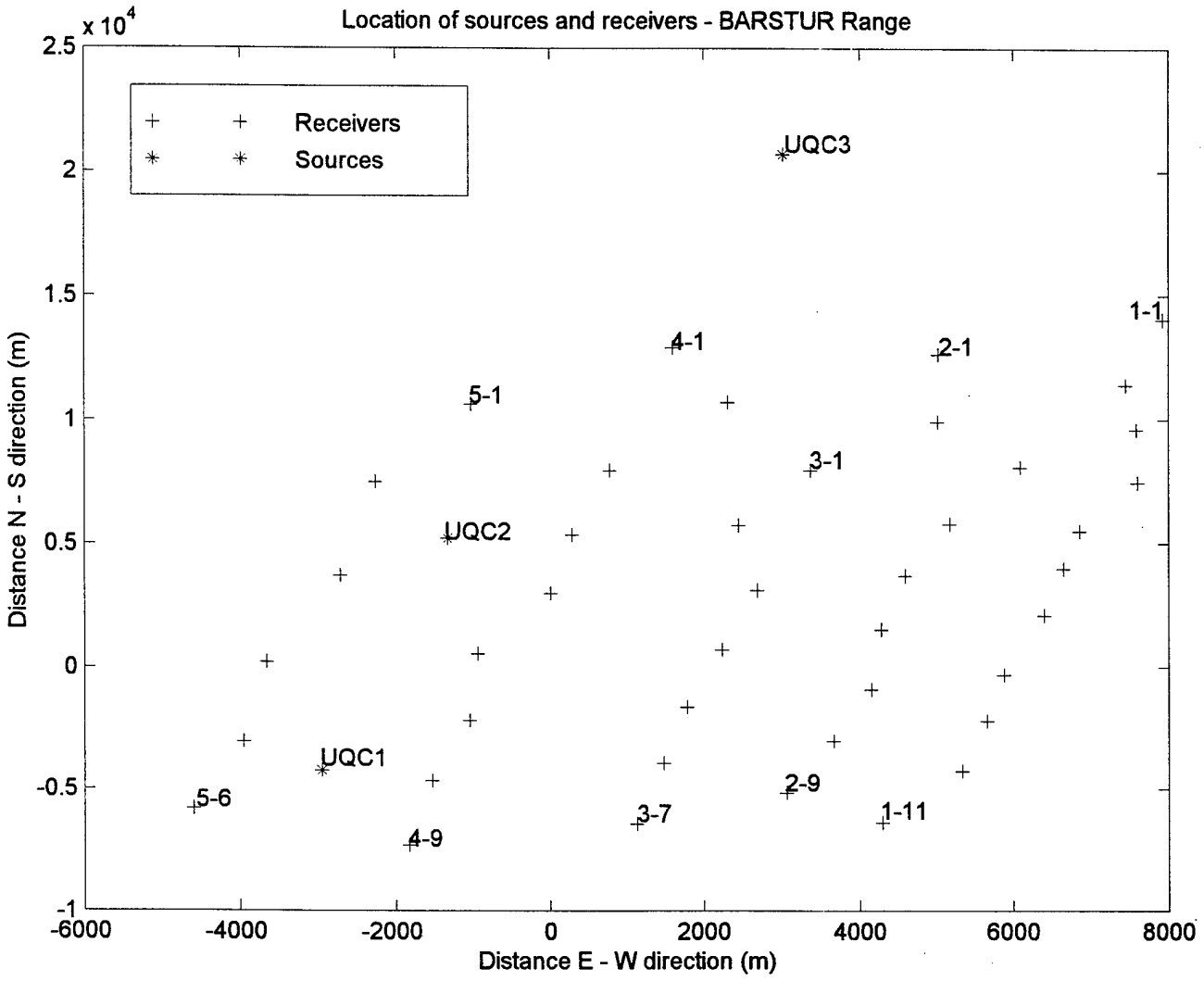

Figure 3. Distribution of sources and receivers at BARSTUR range.

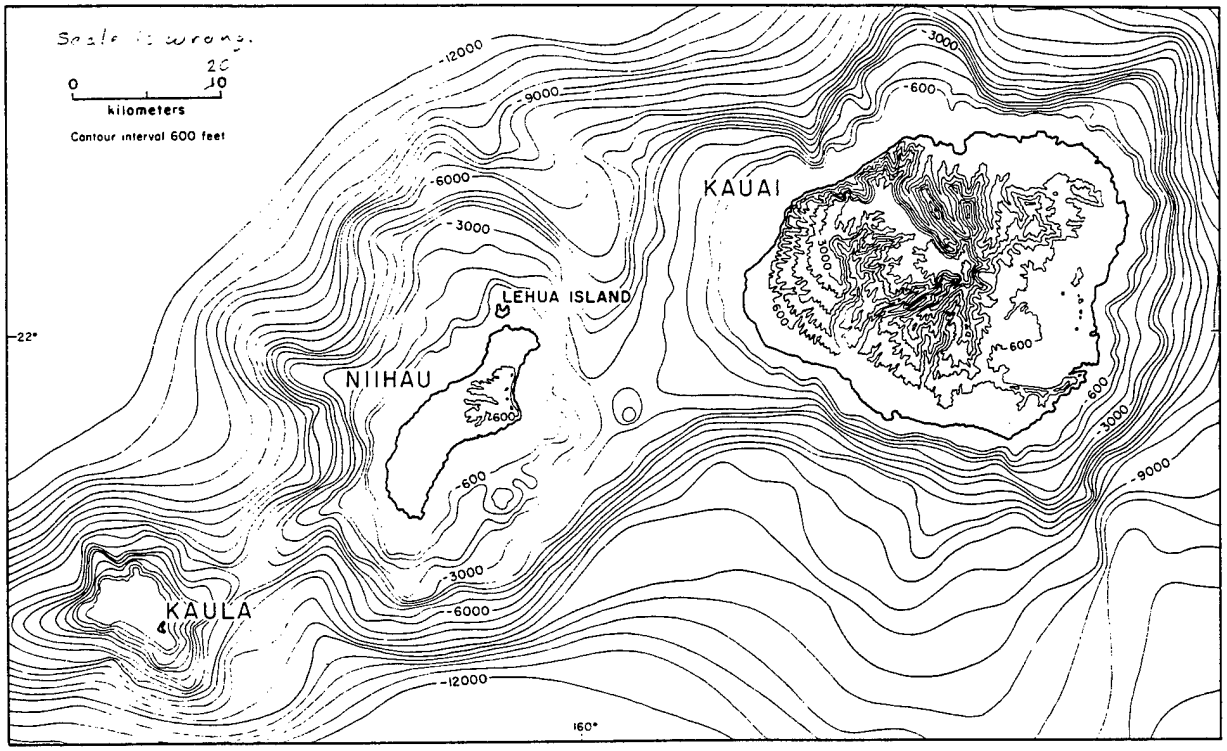

Figure 22.1. Map showing the relationship of Kaula, Niihau, and Kauai and the northeast-trending ridge connecting them. The submarine contours are generalized. (After Stearns, 1947.)

of their excellent exposures along the Napali Coast of northwestern Kauai (figs. 22.6, 22.7). The Napali Formation consists of thin flows of tholeiitic basalt, olivine basalt, and oceanite pahoehoe and aa sloping gently outward in all directions from the summit area. Because of the great amount of erosion of the surface of the shield, very few vents of the Napali Formation are preserved, although the lavas are cut by hundreds of dikes, most of which probably fed flows. Near the top of the west wall of Waimea Canyon, 0.5 kilometer south of the lookout point, a pit crater 0.4 kilometer across and nearly 90 meters deep in the Napali lavas is filled with breccia cut by dikes. It probably was buried by Napali lavas which have been removed by erosion. Masses of breccia near the head of Nualolo Valley, and in the southeast wall of Honopu Valley 0.5 to 0.8 kilometer above its mouth, also may be fillings of pit craters.

Puu Lua, just west of the rim of Waimea Canyon, is the eroded remnant of a crater filled with talus breccia which is capped by a thick massive lava flow much like that which fills the eastern end of Makaopuhi Crater on Kilauea volcano. The massive crater fill is more resistant to erosion than are the surrounding thin-bedded lavas, and removal of the surrounding rocks has left it standing 60 meters above the ground around it. Puu ka Pele, at the rim of Waimea Canyon 1.5 kilometers southeast of Puu Lua, also appears to be a remnant of a resistant, crater-filling lava flow that has been left standing in high relief by the erosion of the less resistant

from G.A. Macdonald, A.T. Abbott, and F.L. Peterson (1983) Volcanoes in the Sea: University of Hawaii Press, page 454

Figure 4. Bathymetry of regions surrounding the Hawaii Islands.

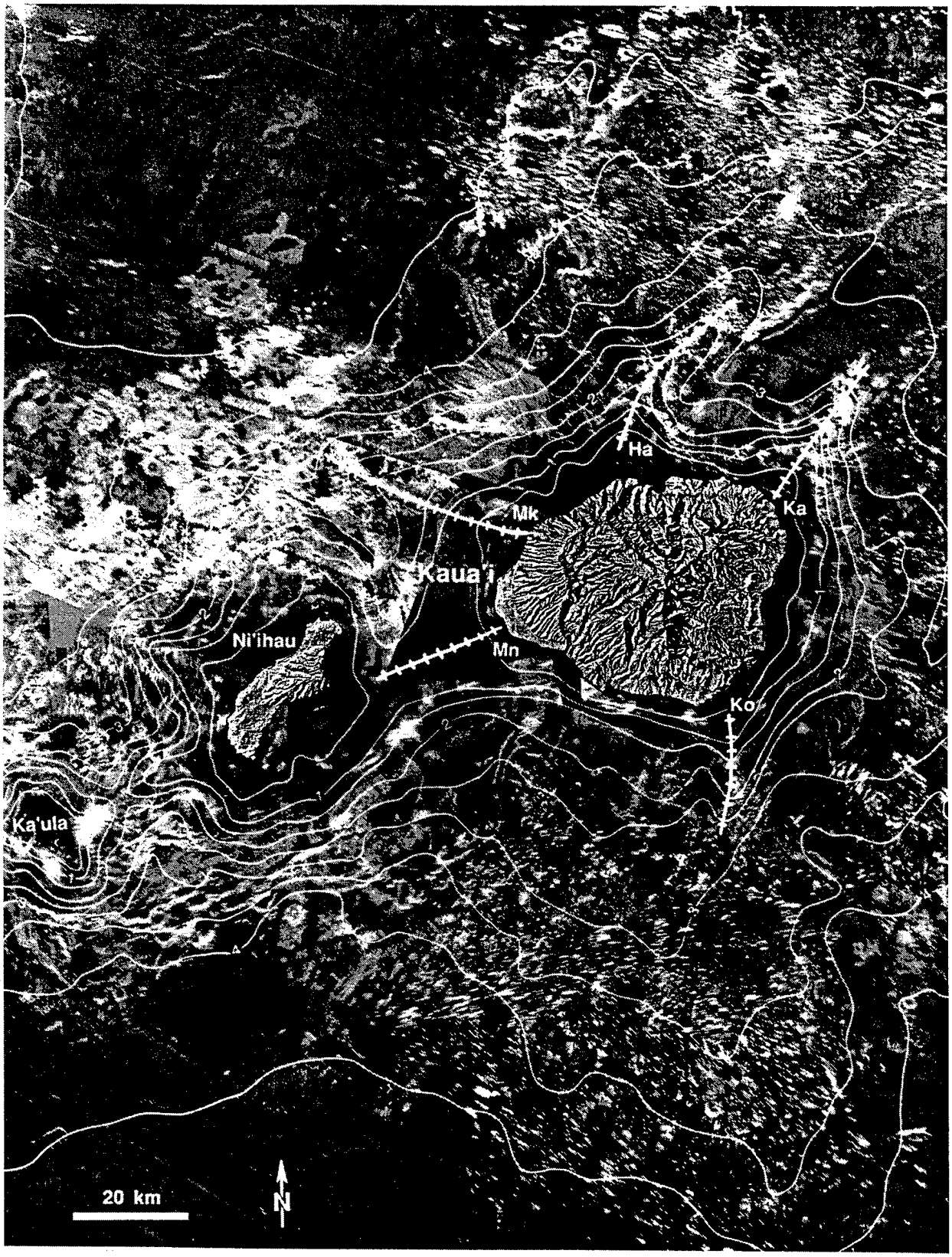

Figure 5. Side scan sonar image of region around Kauai.

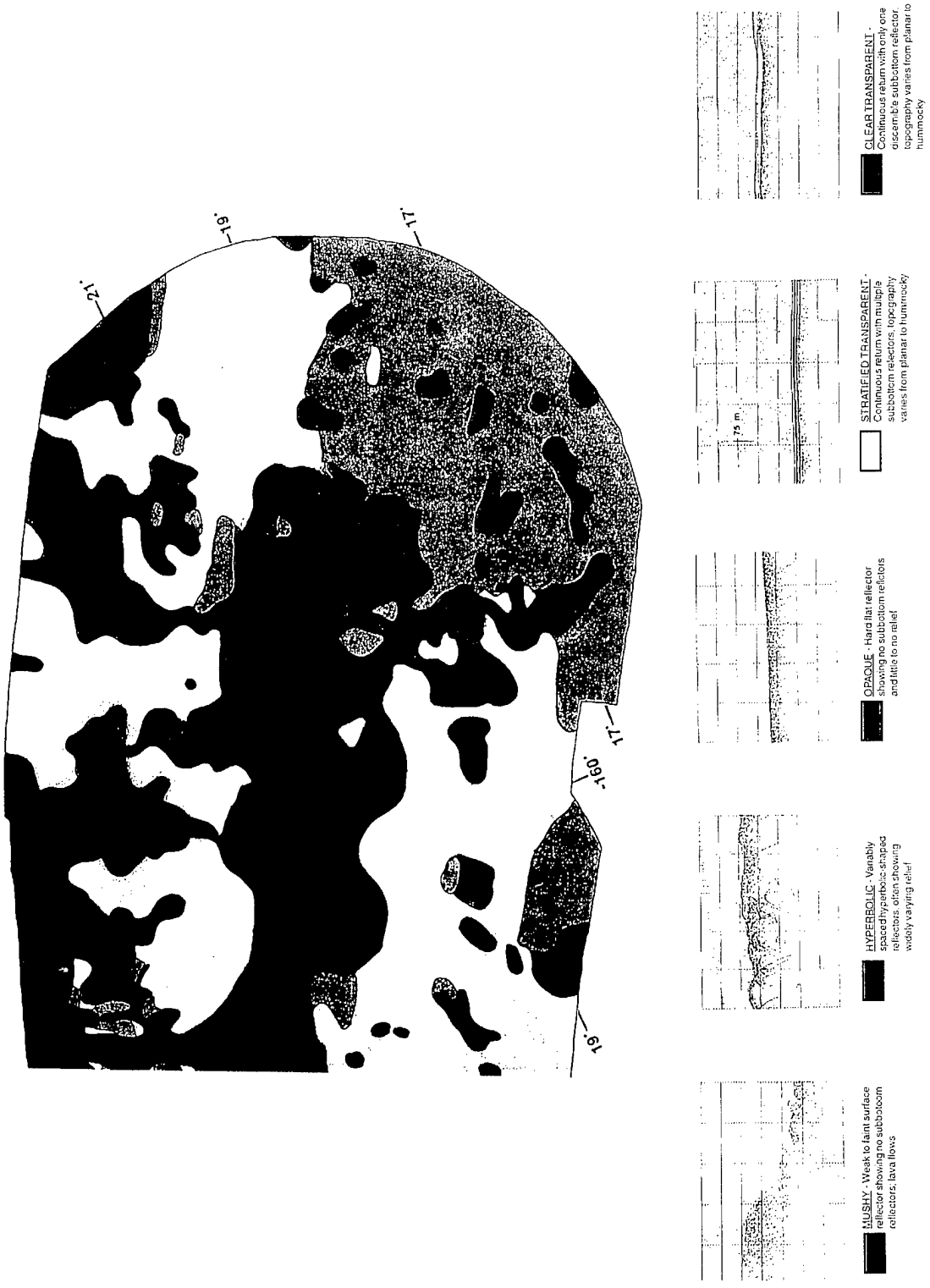

Figure 6. Sediment characterization of regions around Kauai.

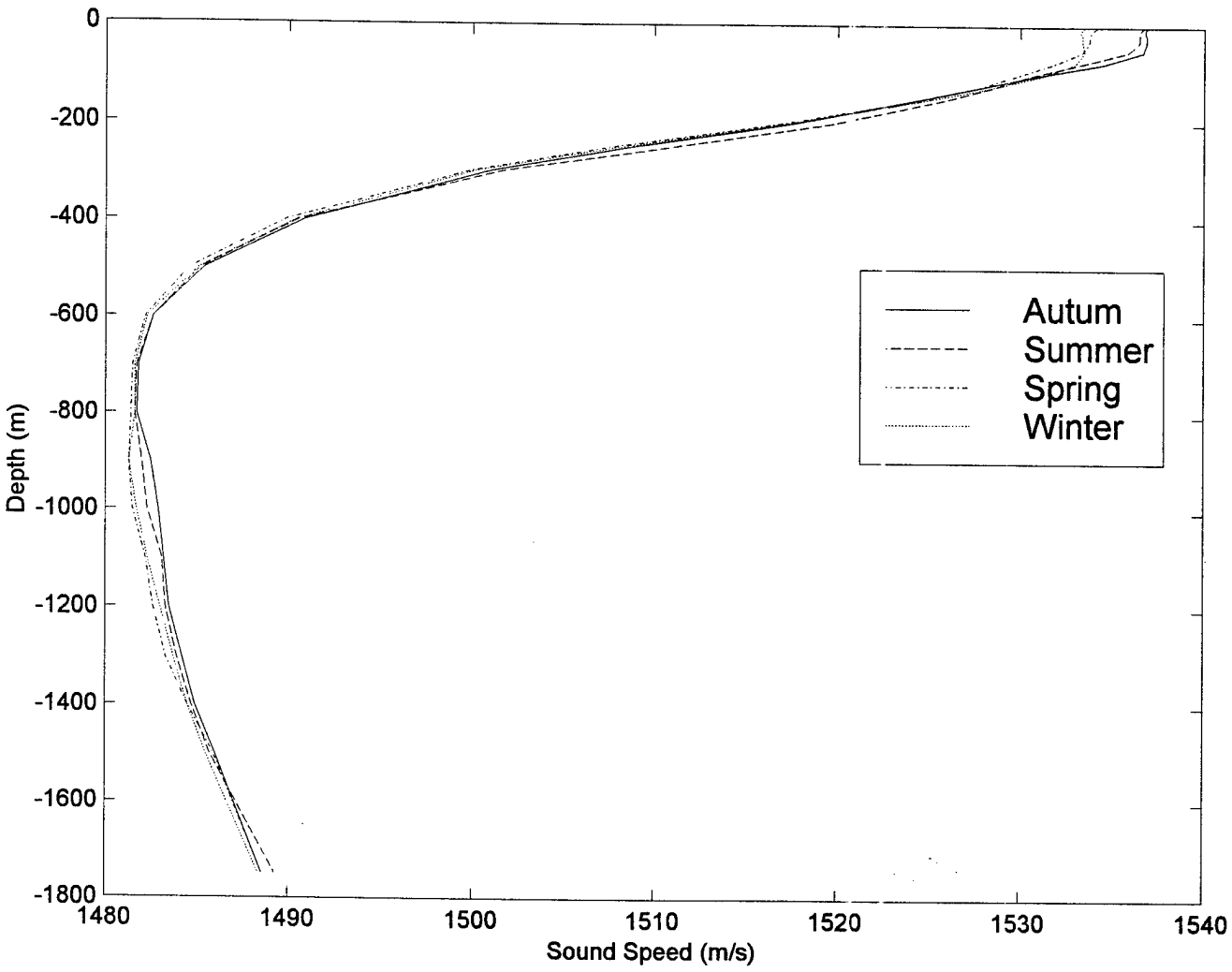

Figure 7. Average sound speed profiles for the four seasons in the PMRF region.

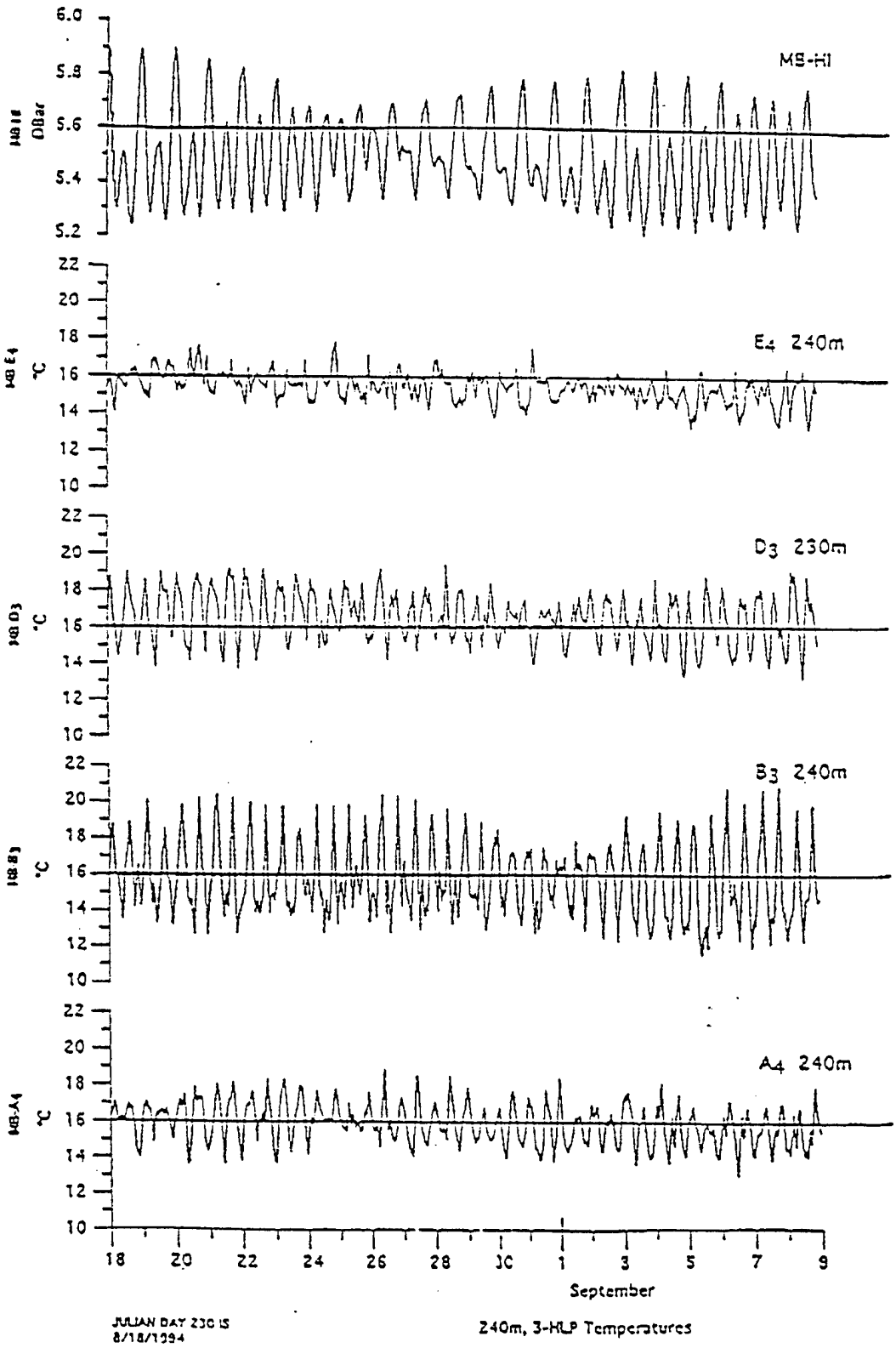

Figure 8. Temperature at 240 m for the offshore mooring. Top panel shows the water-level (pressure) record for Hickam Harbor.

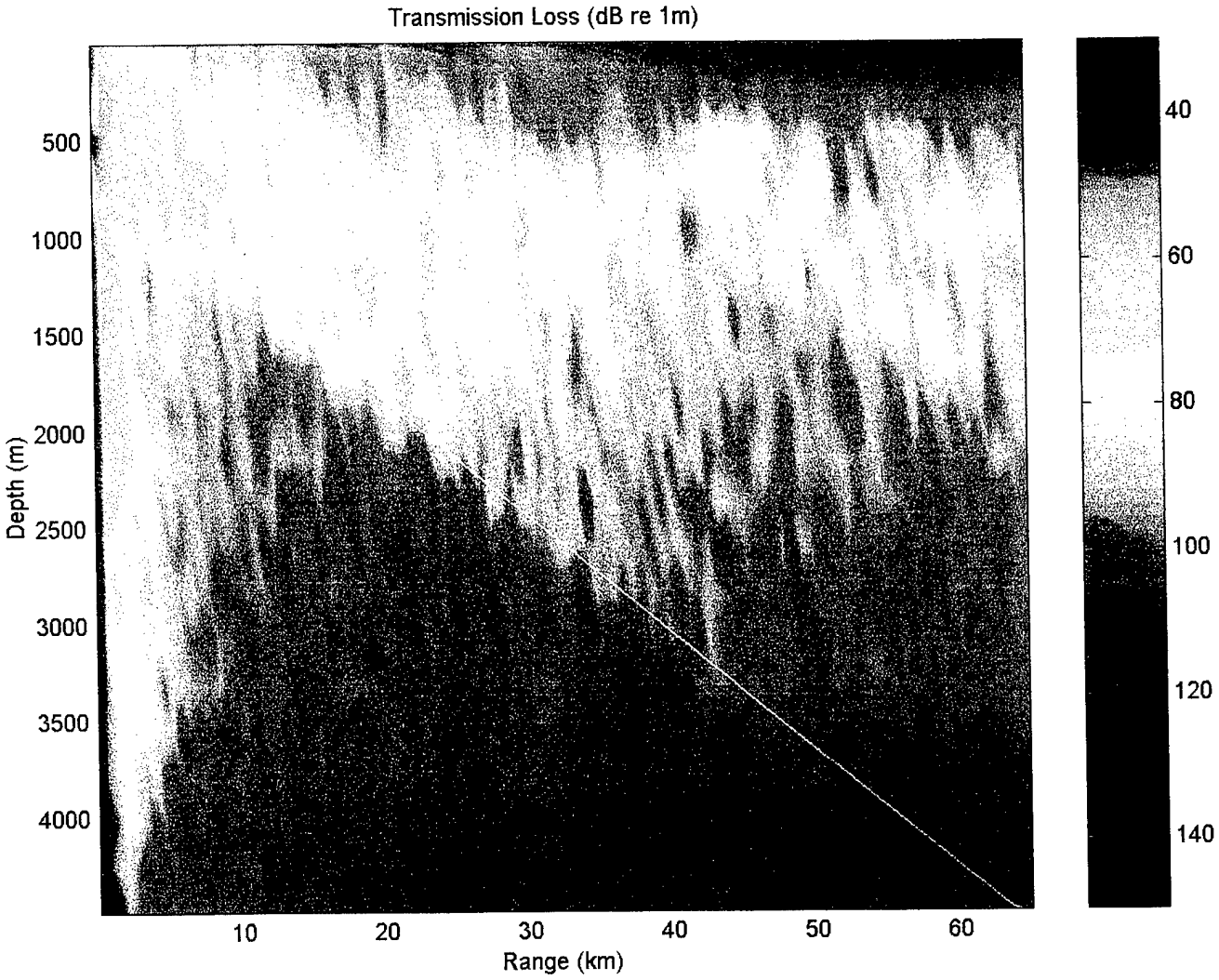

Figure 9. Down slope propagation. Source depth = 500 m, Frequency = 1000 Hz.

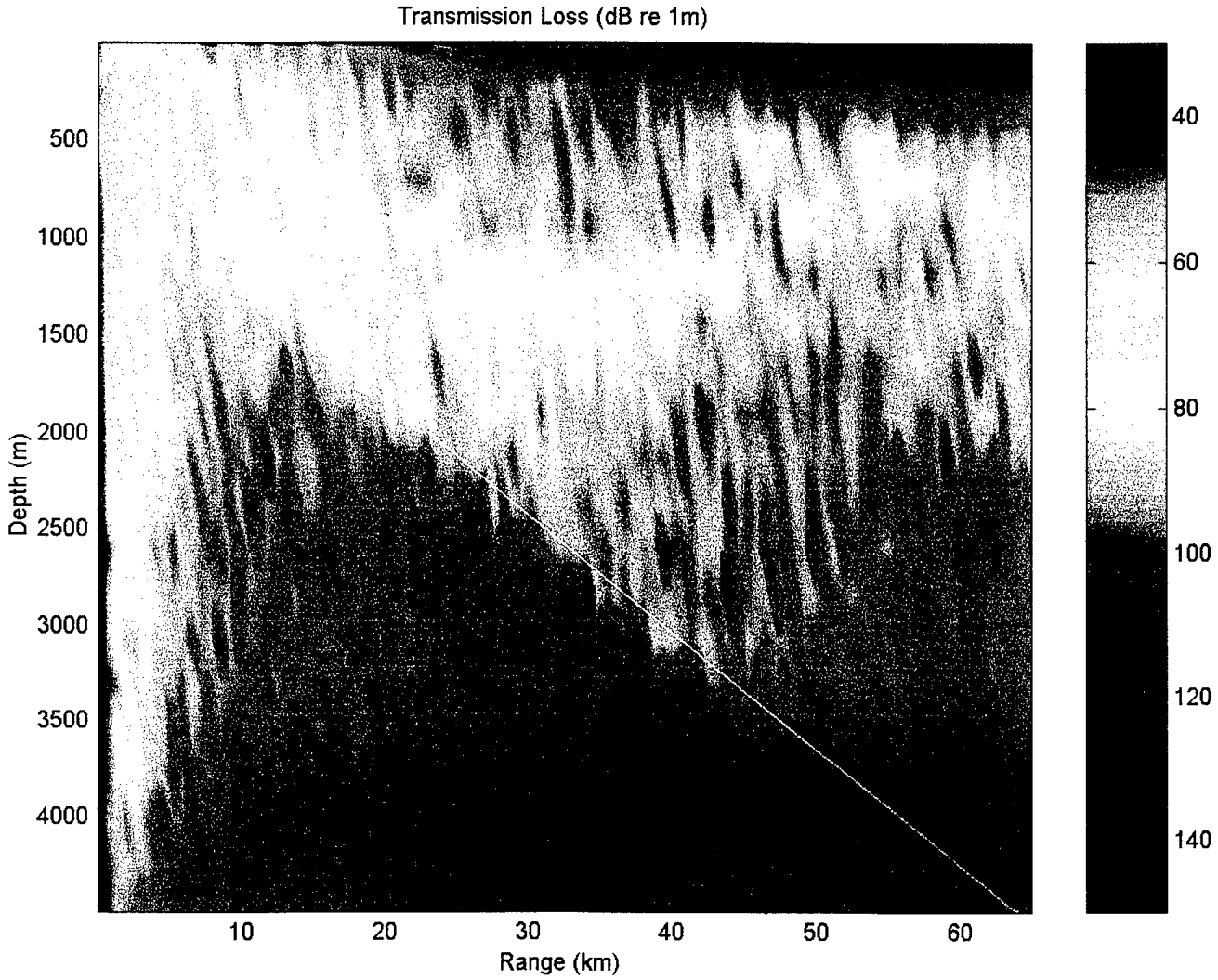

Figure 10. Down slope propagation. Source depth = 250 m. Frequency = 1000 Hz.

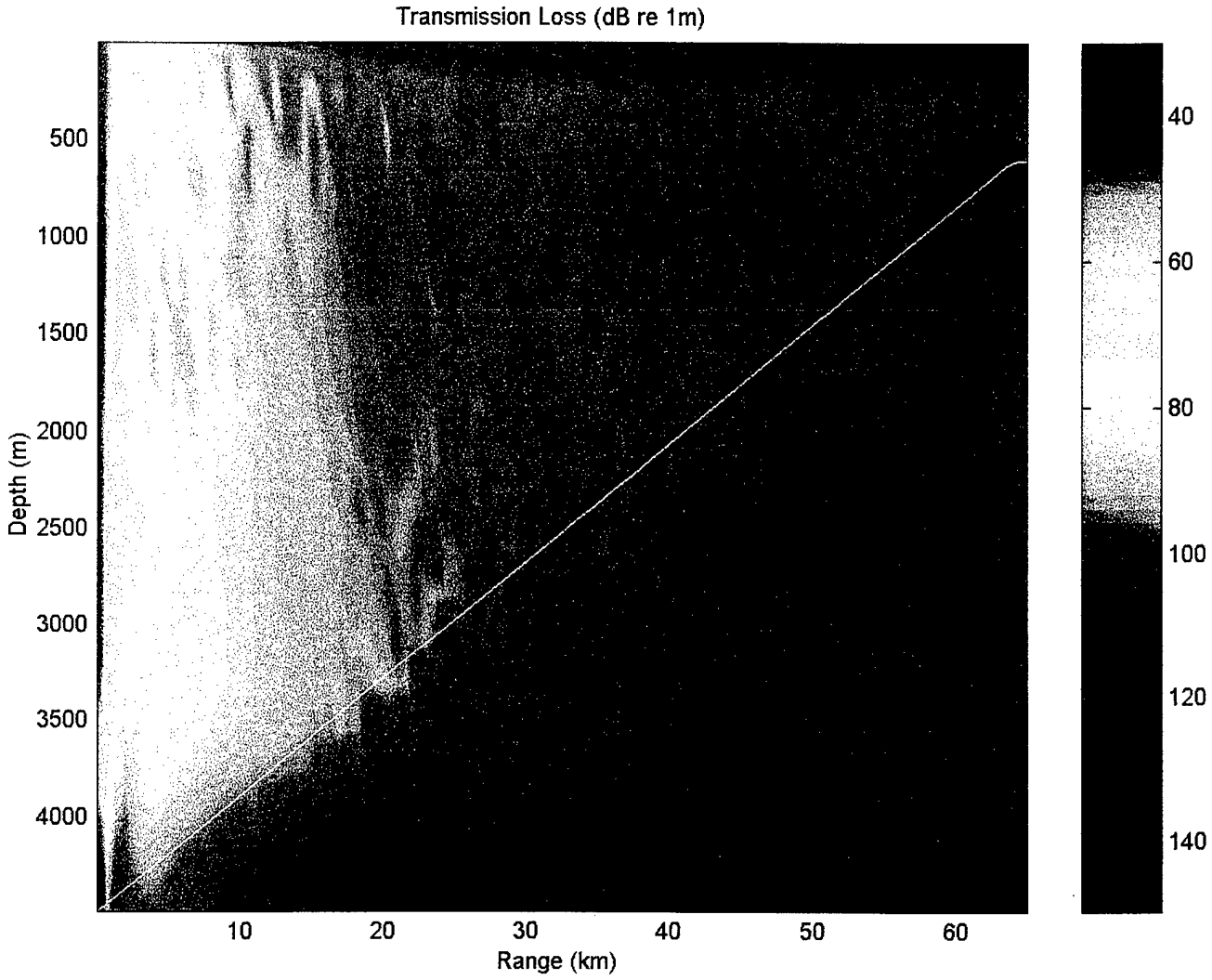

Figure 11. Up slope propagation. Source depth = 3500 m. Frequency = 1000 Hz.

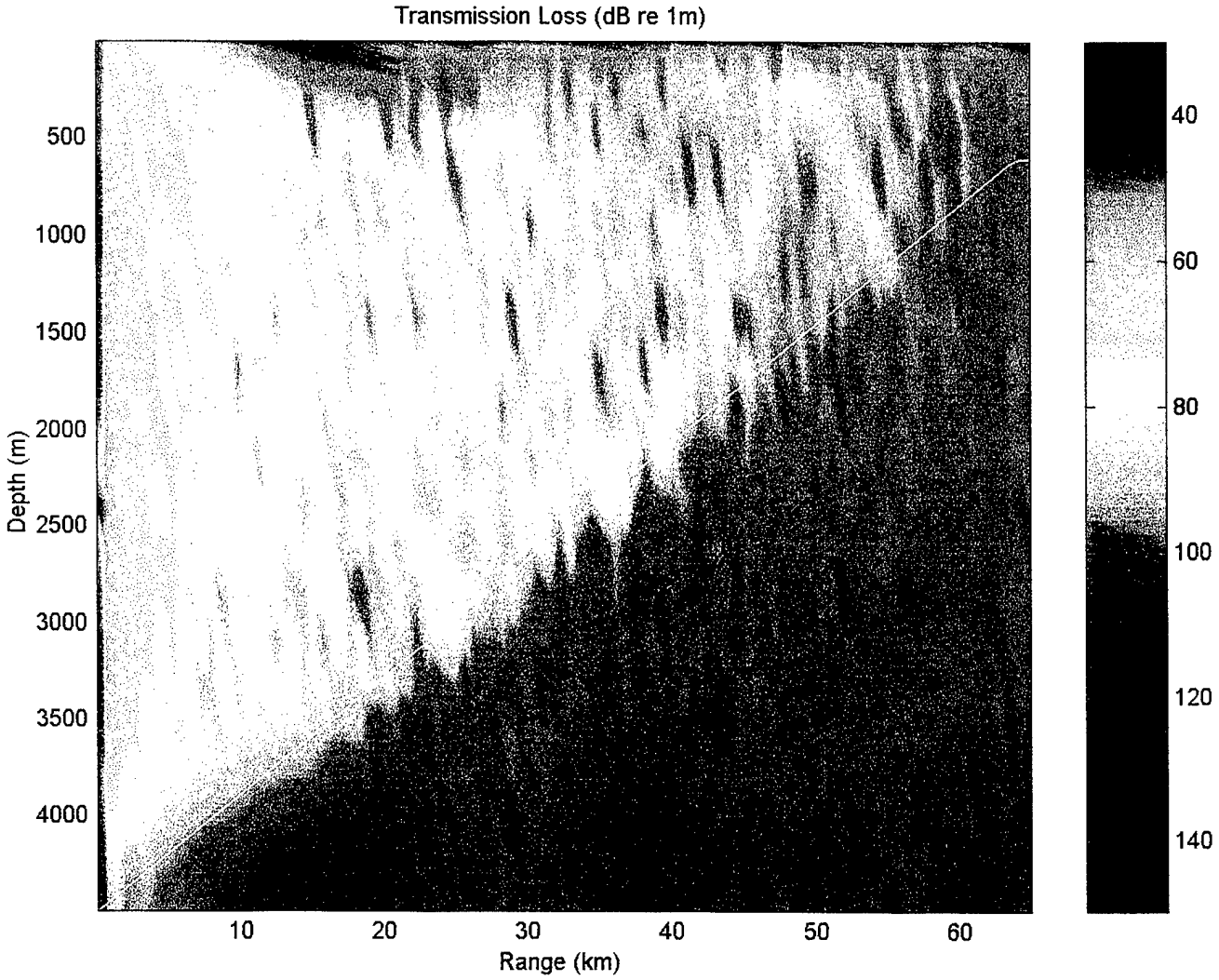

Figure 12. Up slope propagation. Source depth = 2200 m. Frequency = 1000 Hz.

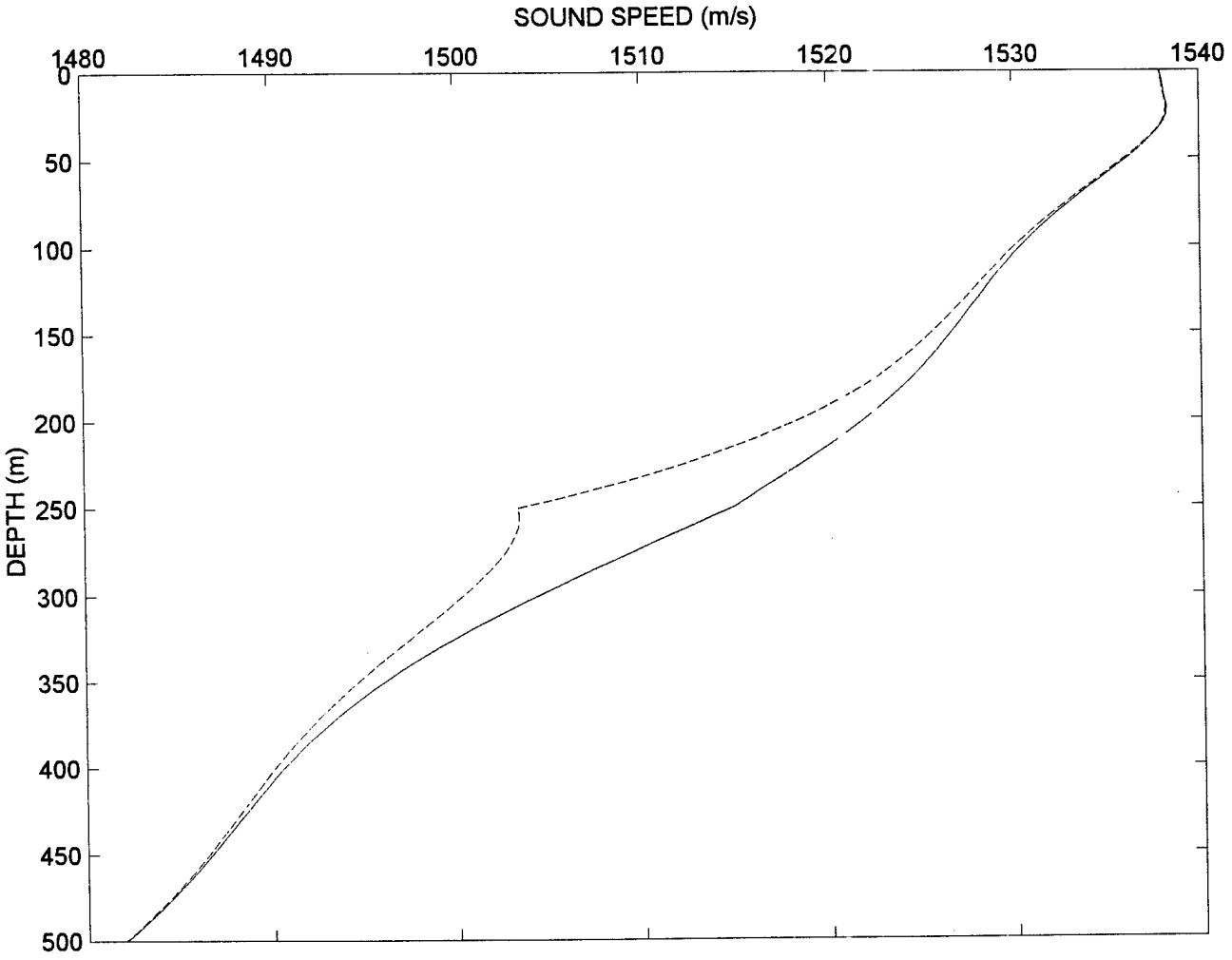

Figure 13. Sound speed fluctuation due to internal tides. The dotted profile shows the fluctuations in sound speed as a result of internal tides. These two profiles will be referred to INT1 and INT2 in succeeding plots.

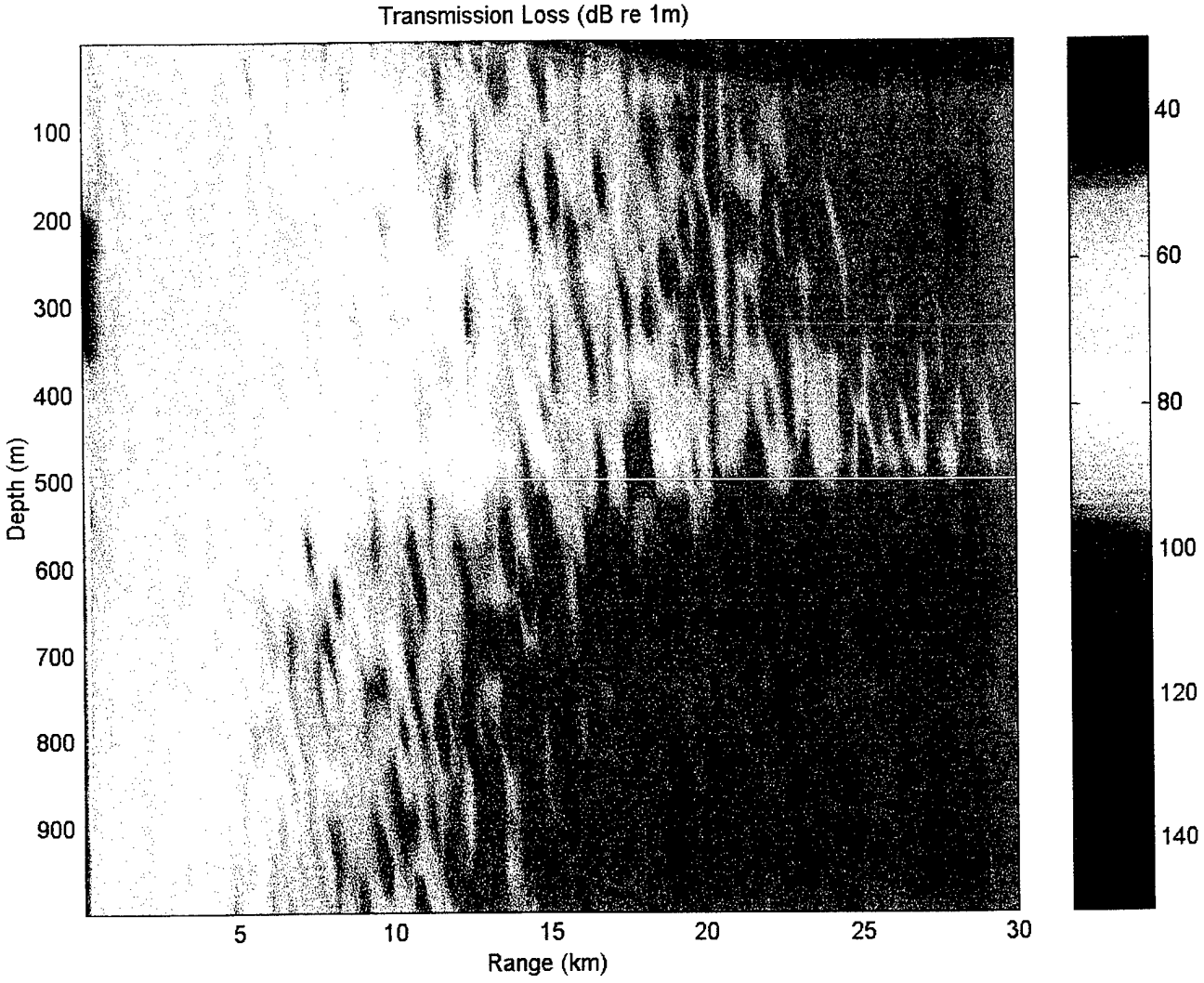

Figure 14. Transmission loss plot for profile INT1. Source depth = 250 m. Freq. = 1000 Hz.

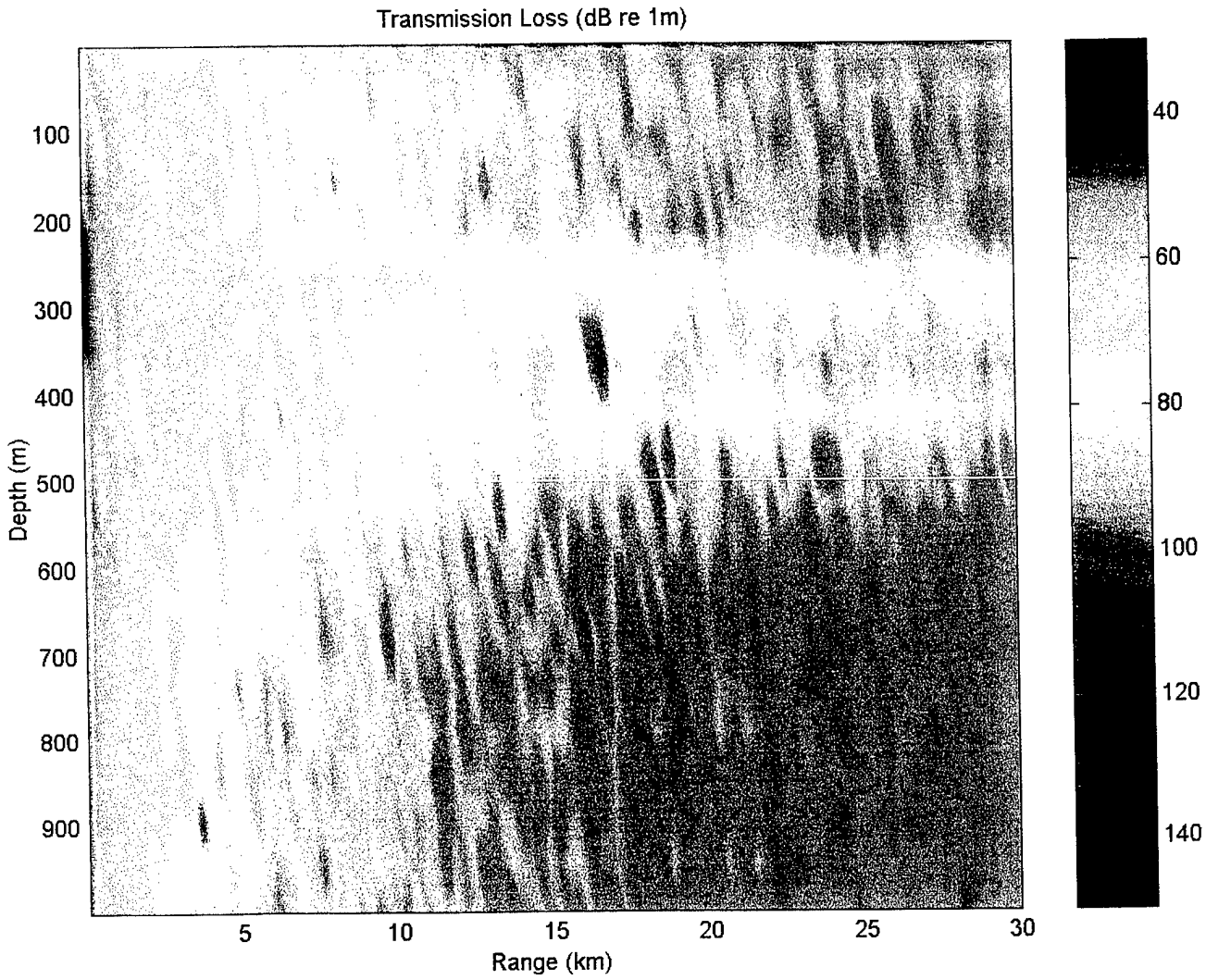

Figure 15. Transmission loss plot for profile INT2. Source depth = 250 m. Freq. = 1000 Hz.

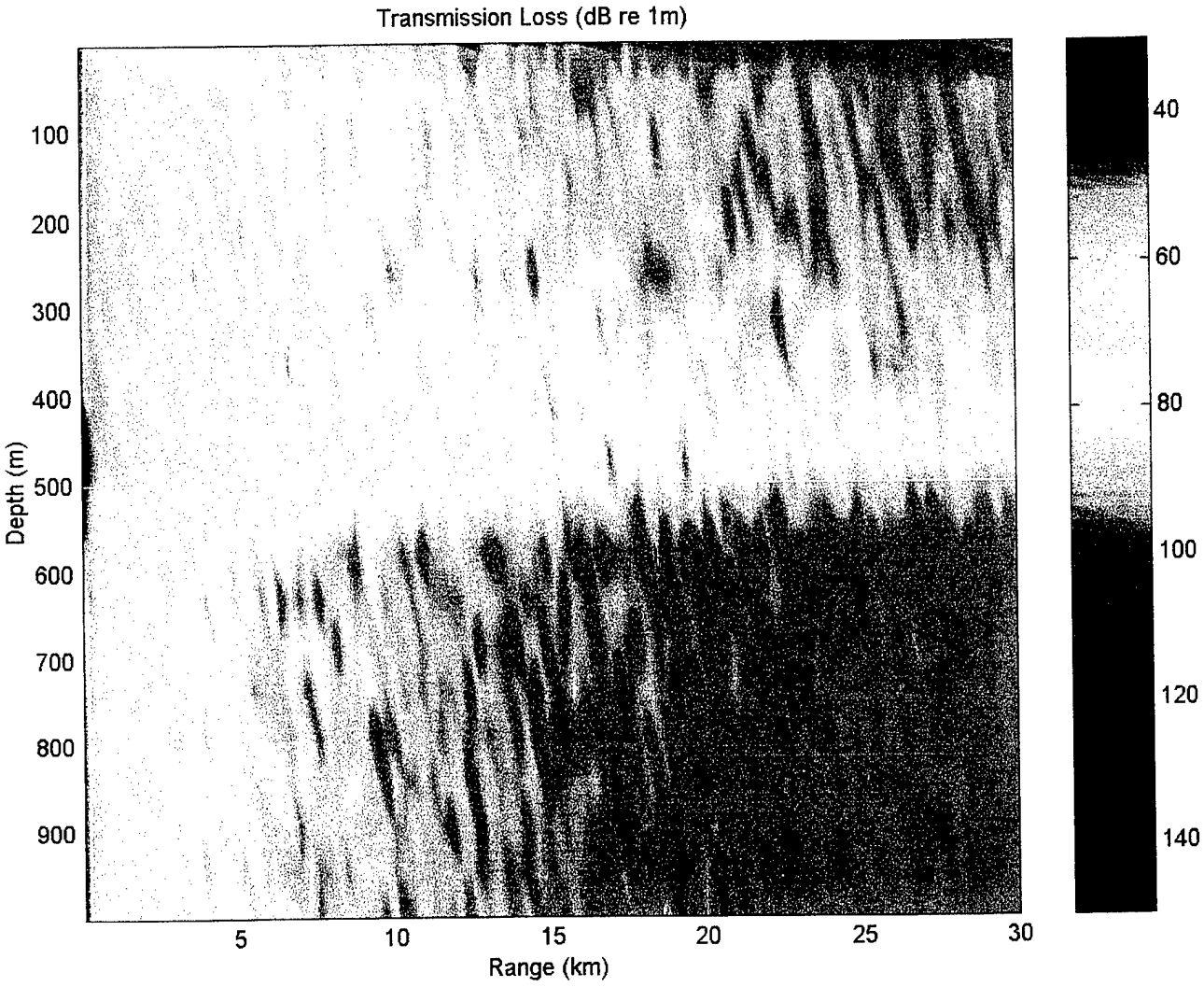

Figure 16. Transmission loss plot for profile INT1. Source depth = 450 m. Freq. = 1000 Hz.

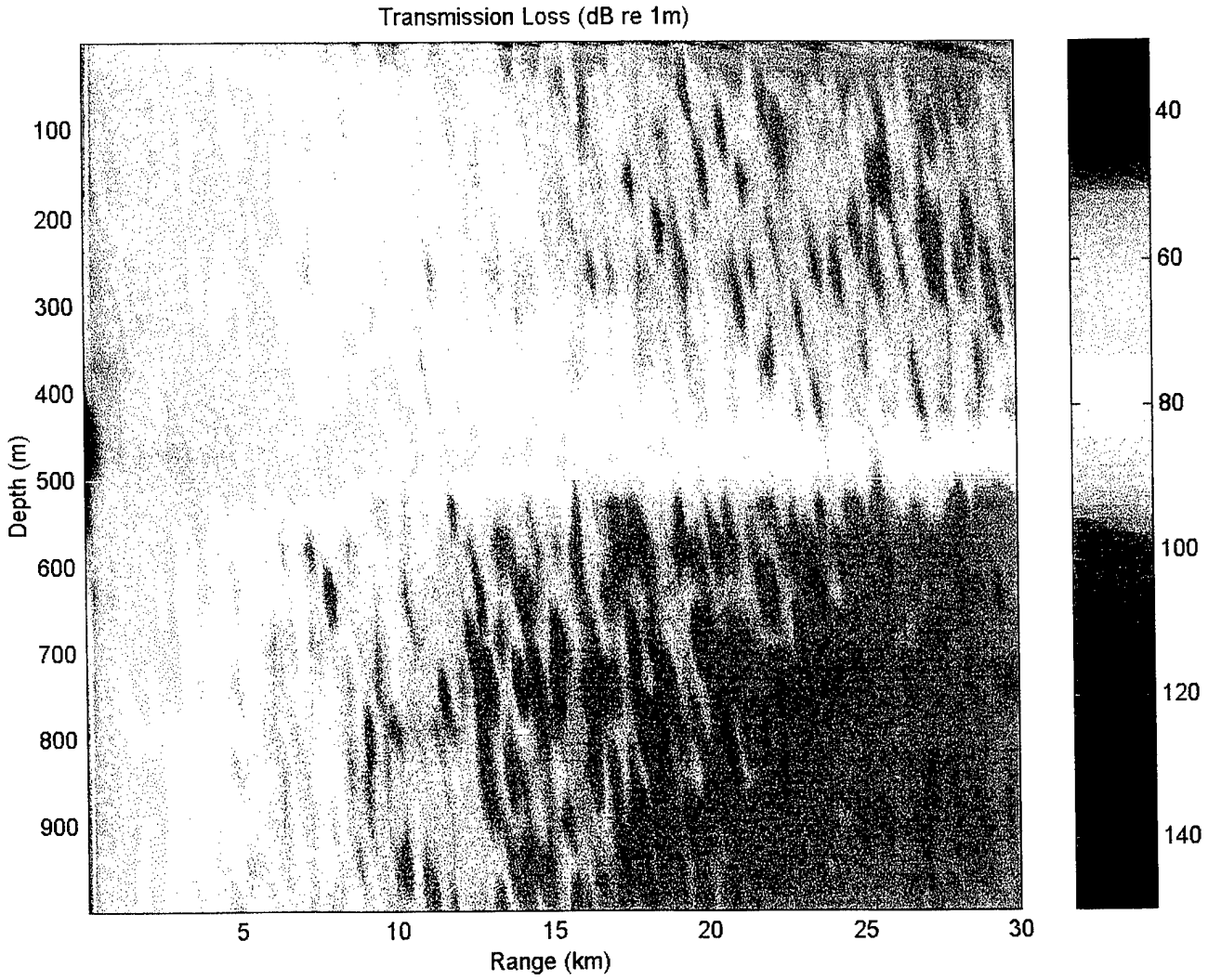

Figure 17. Transmission loss plot for profile INT2. Source depth = 450 m. Freq. = 1000 Hz.

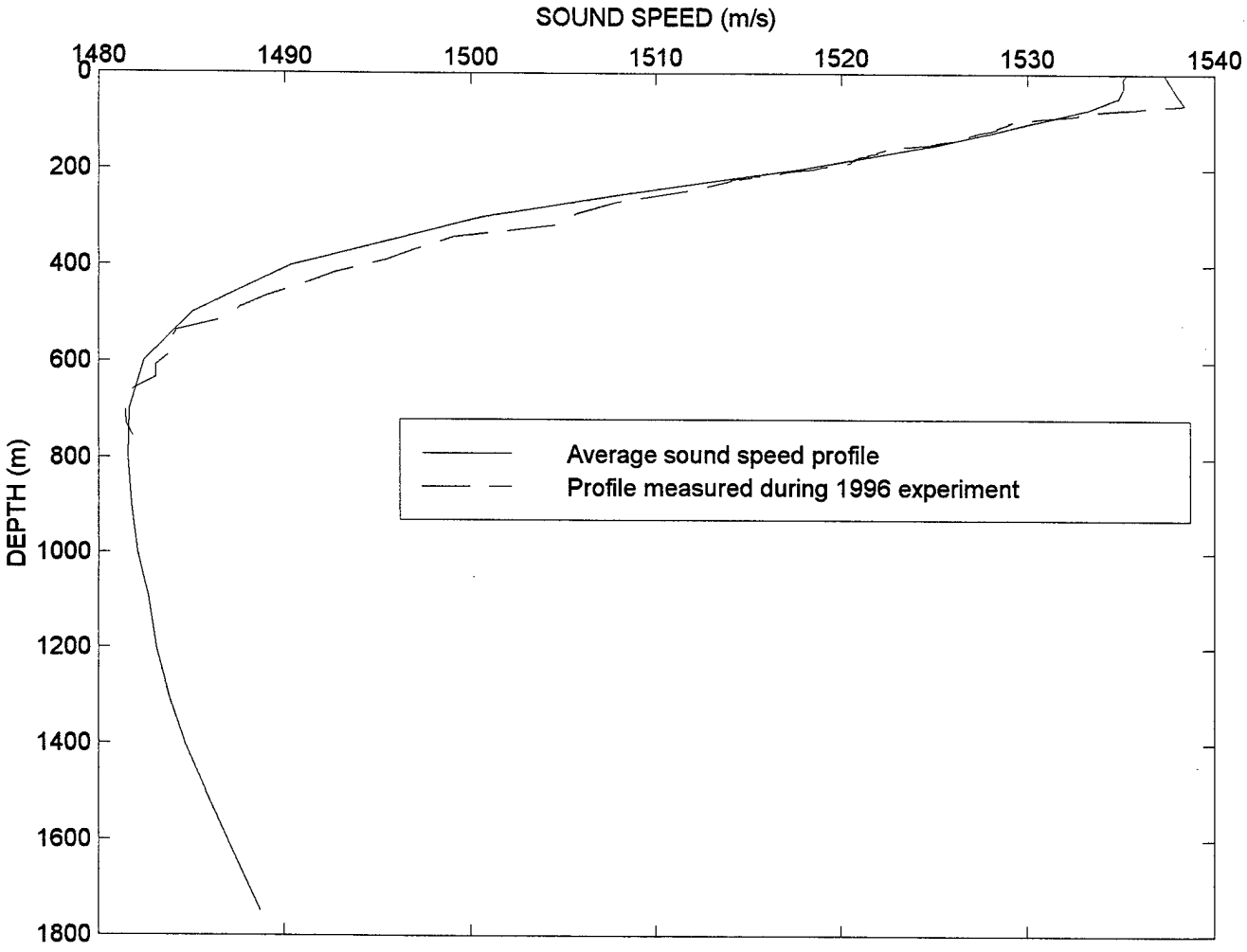

Figure 18. Sound speed profile determined during December 1996 experiment.

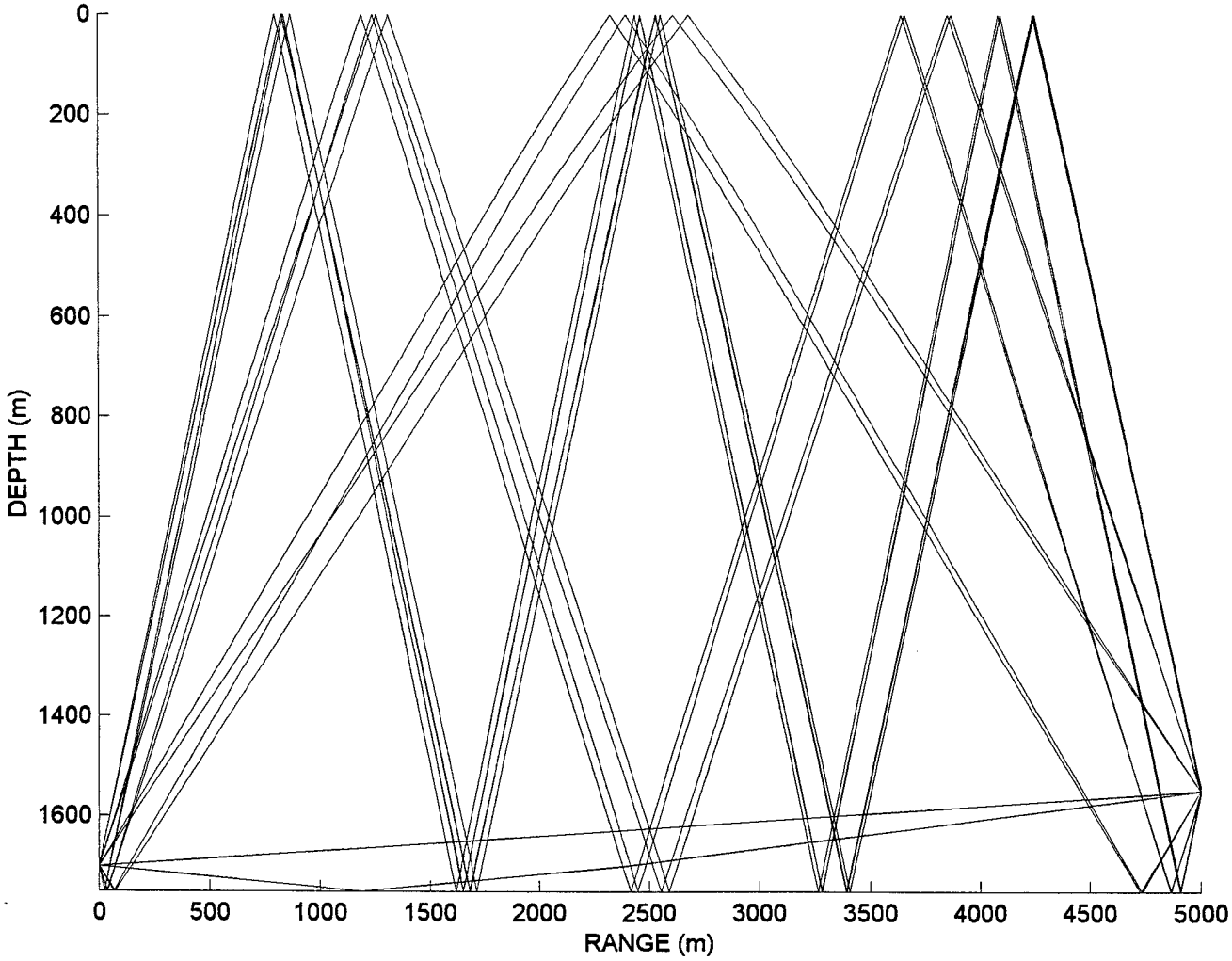

Figure 19. Ray diagram for propagation from UQC1 to receiver 4-6.

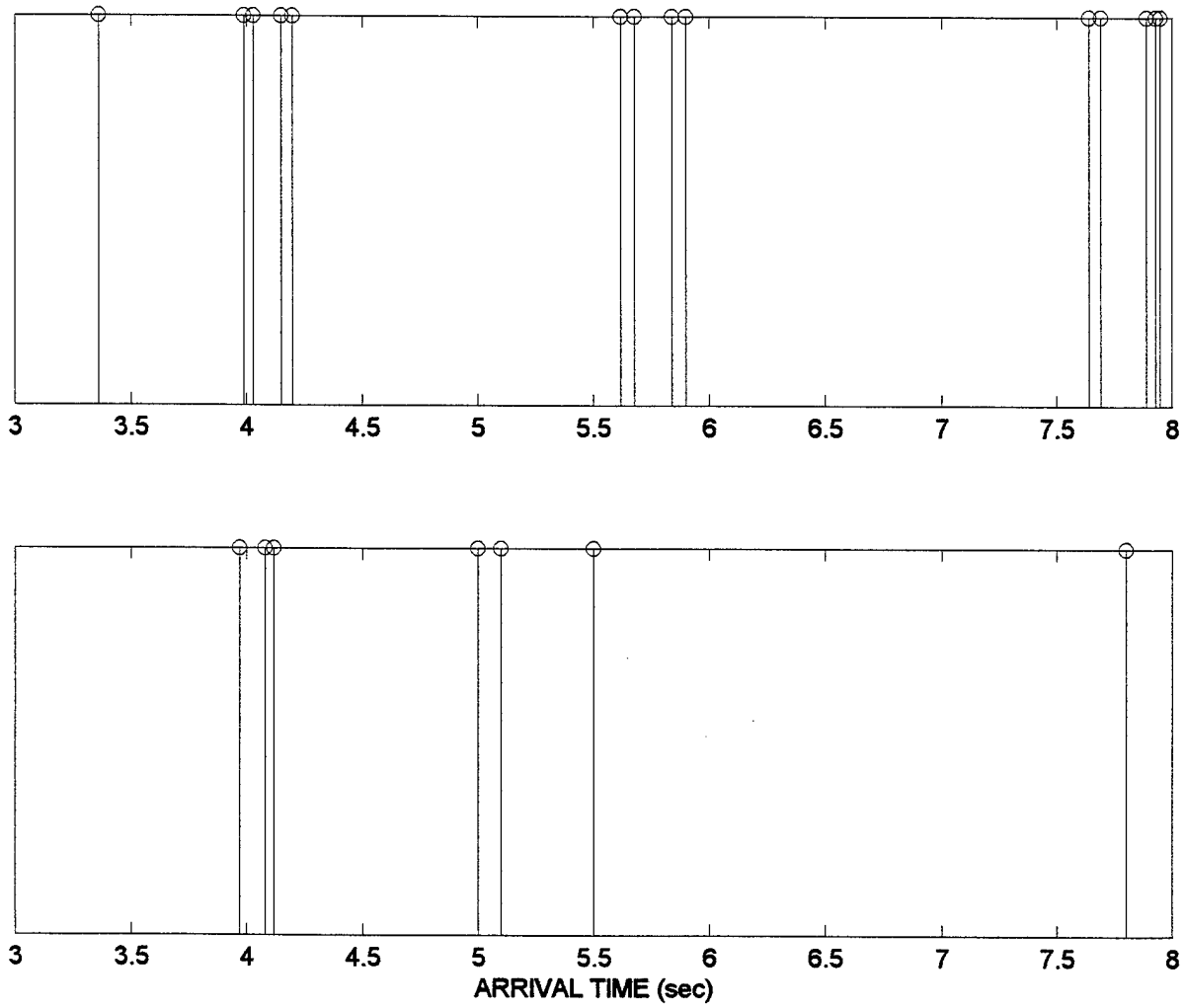

Figure 20. Arrival structure for receiver 4-6. Top: Model prediction. Bottom: Arrival times from data.

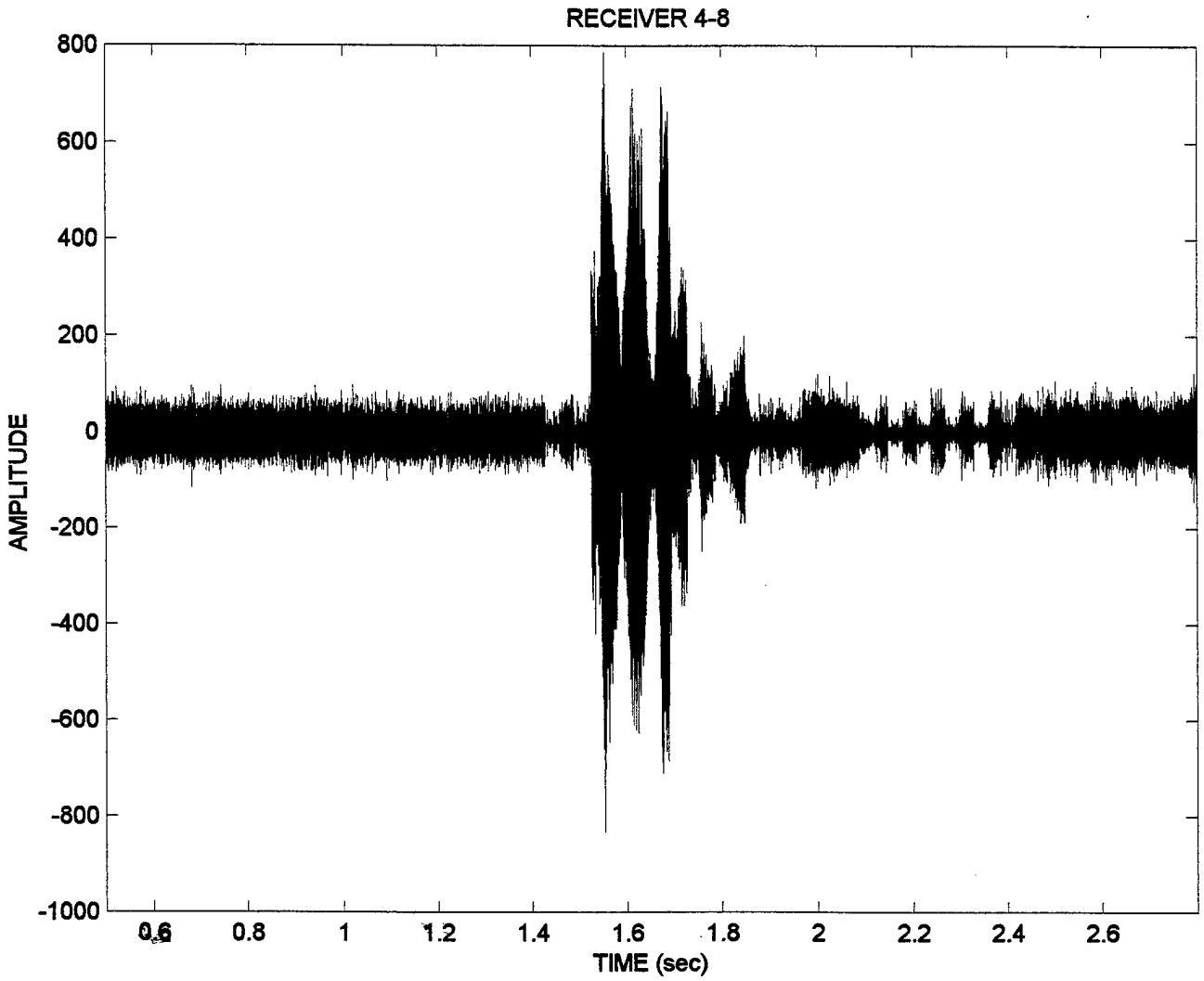

Figure 21. Part of signal received at receiver 4-8. Note from the ray diagram that the arrivals will come in groups.

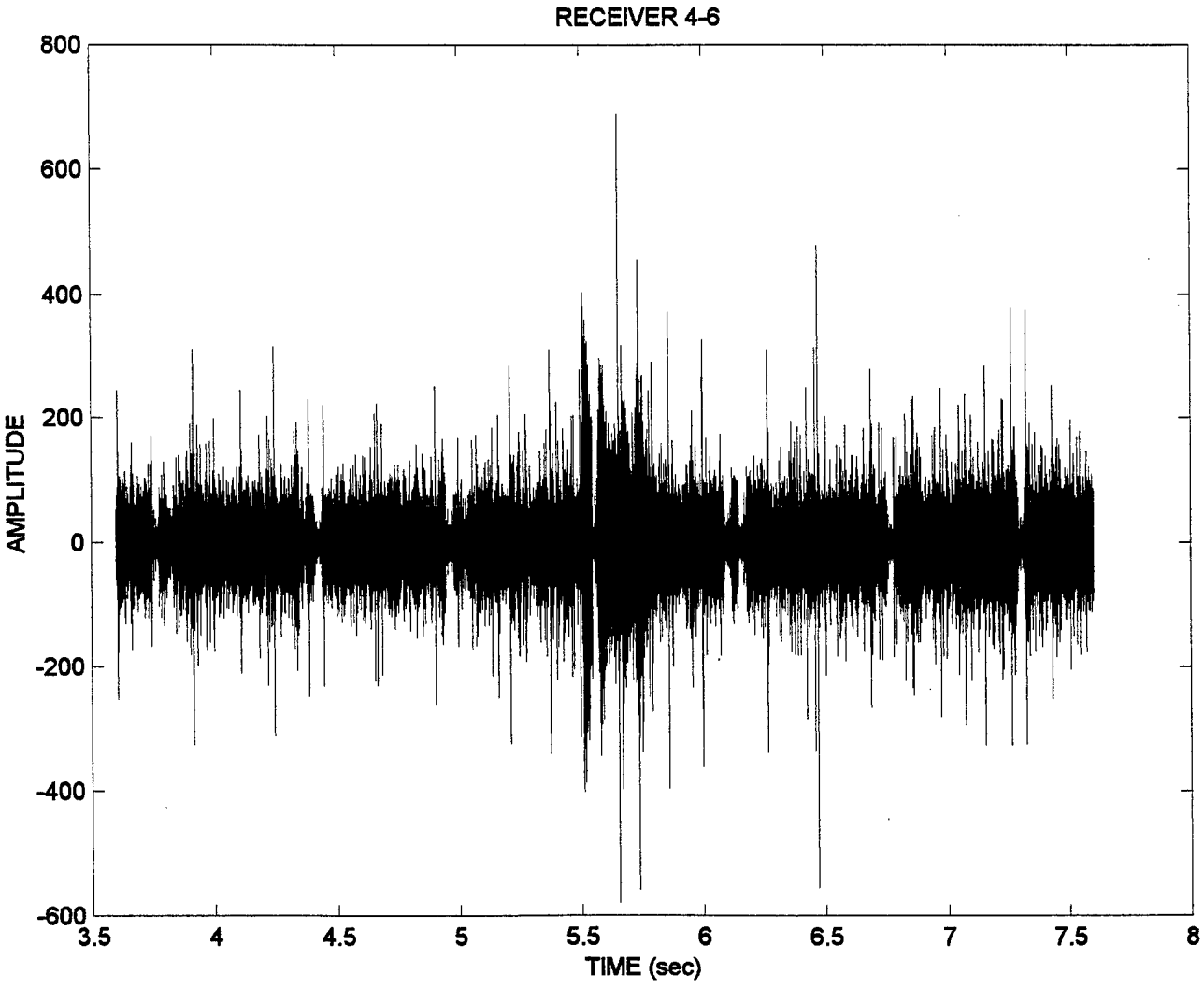

Figure 22. Signal received at receiver 4-6.

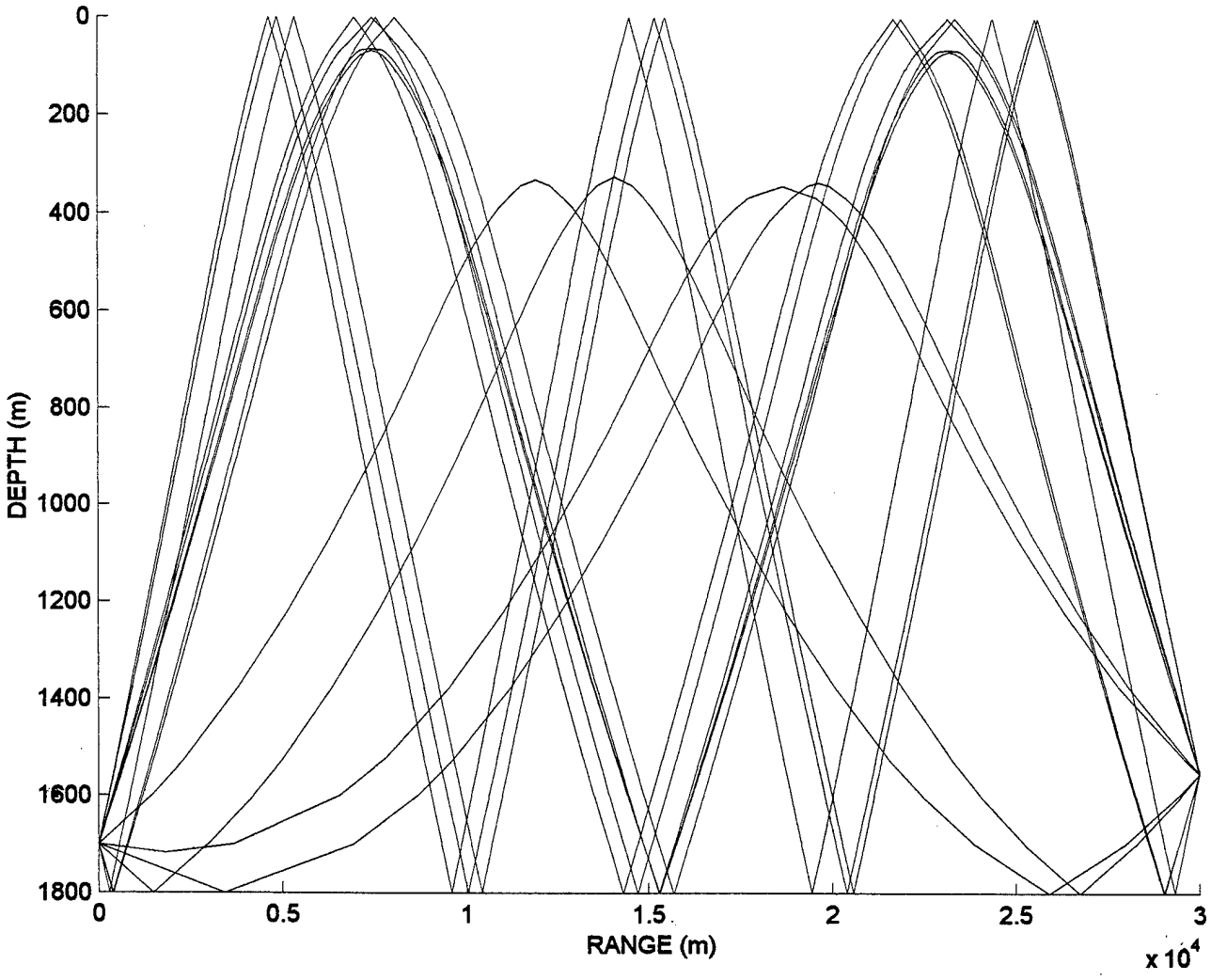

Figure 23. Ray diagram for propagation out to 30 km.

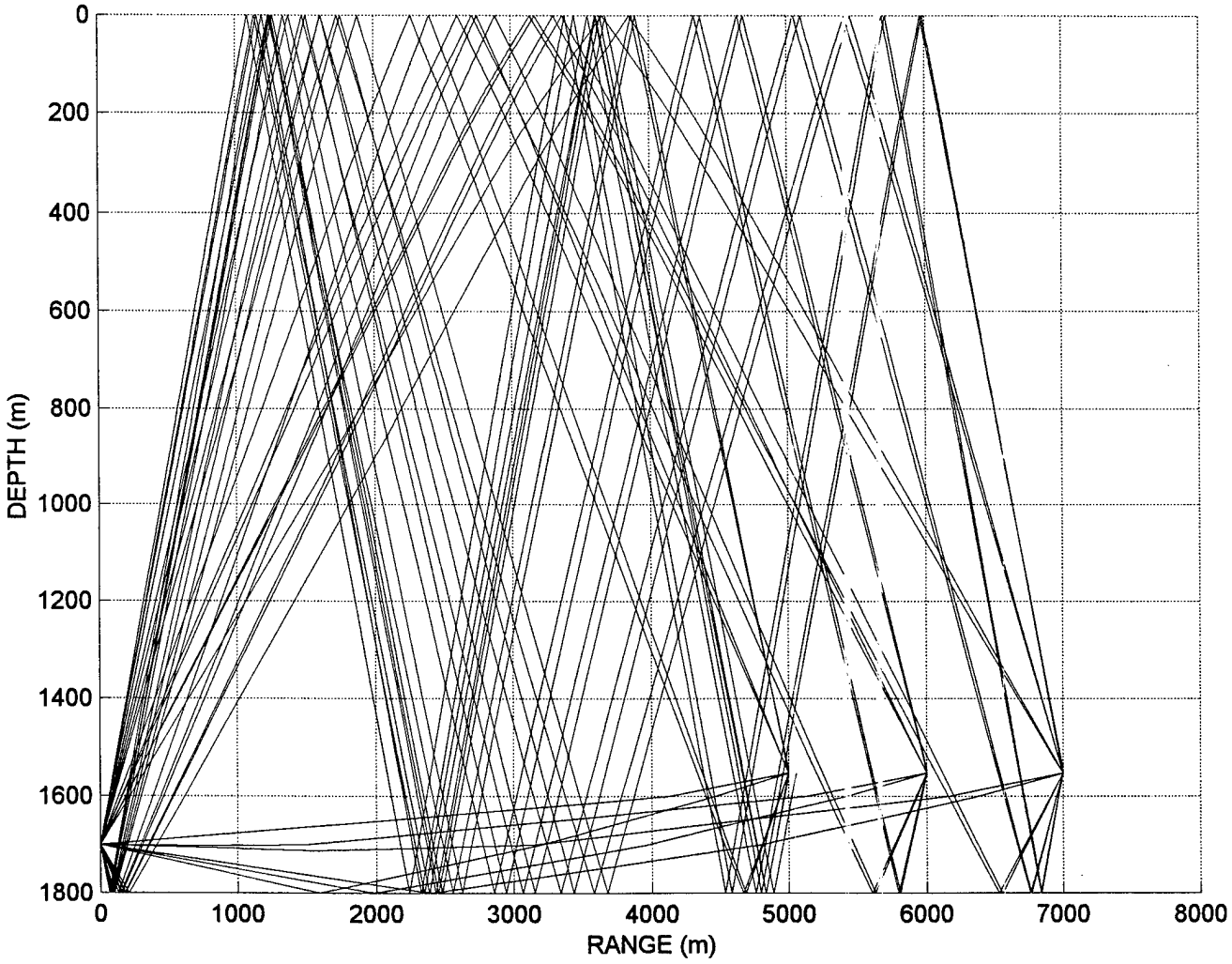

Figure 24. Ray diagram for arrivals at a horizontal array close to the ocean floor.

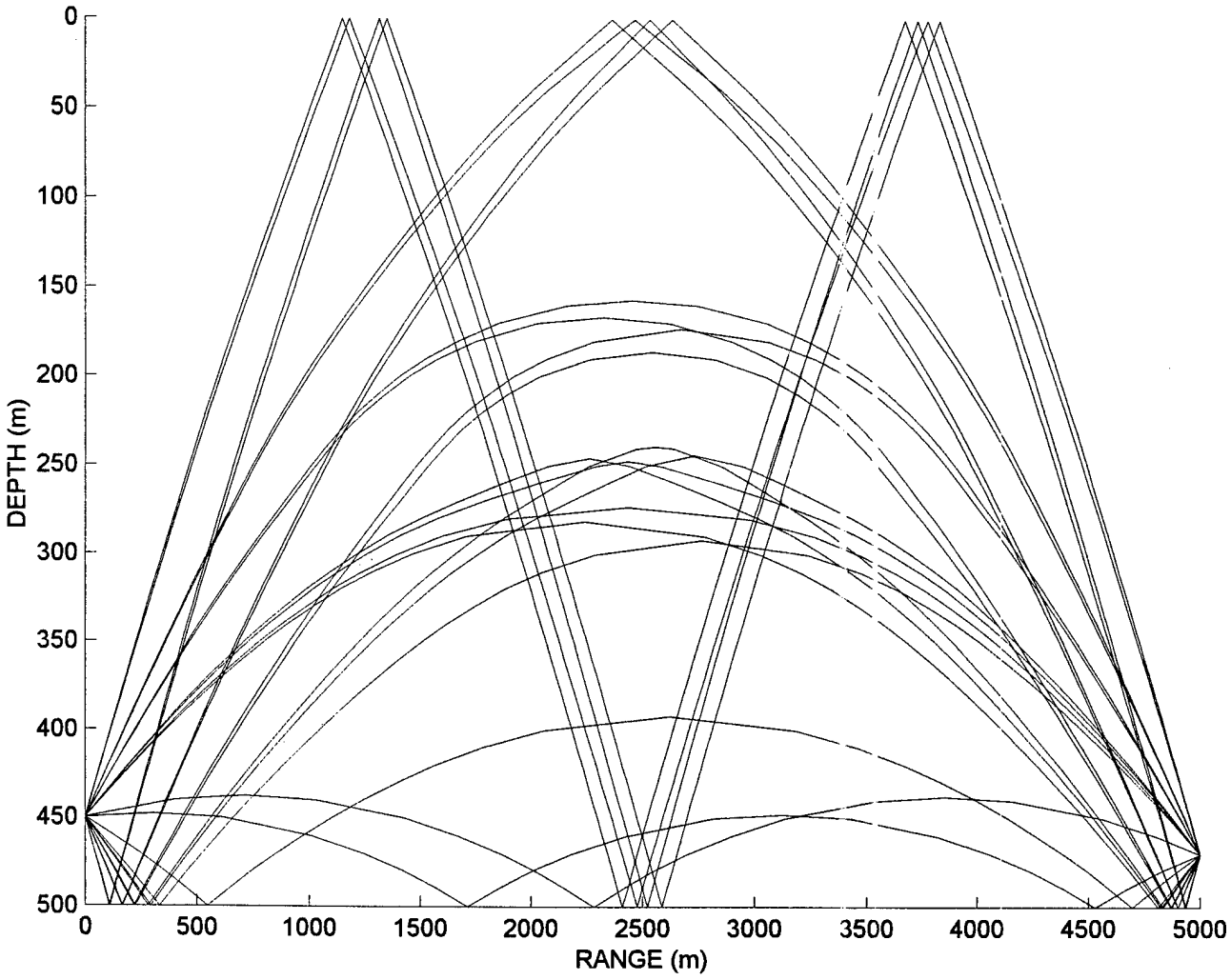

Figure 25. Ray diagram for starting profile.

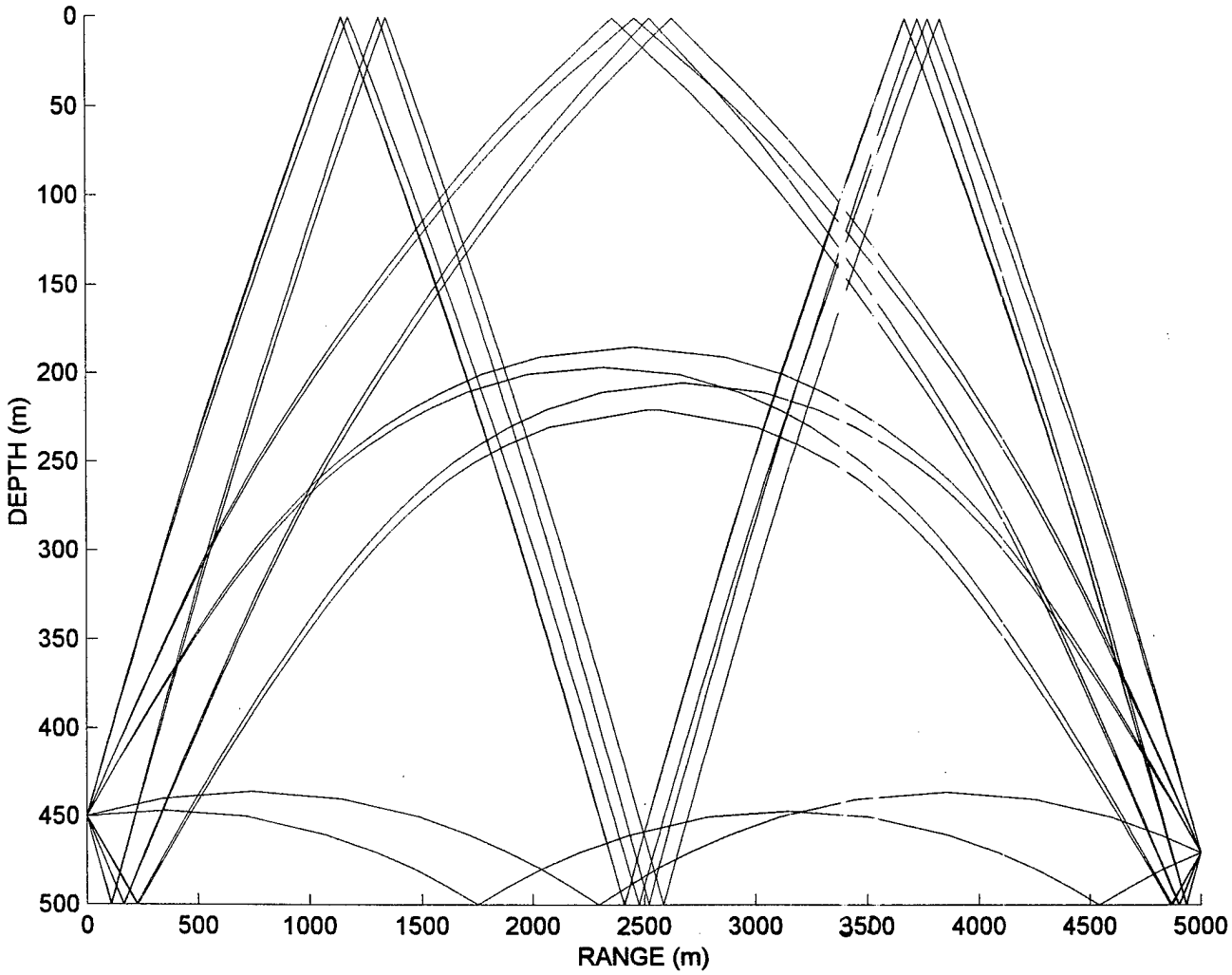

Figure 26. Ray diagram for target profile.

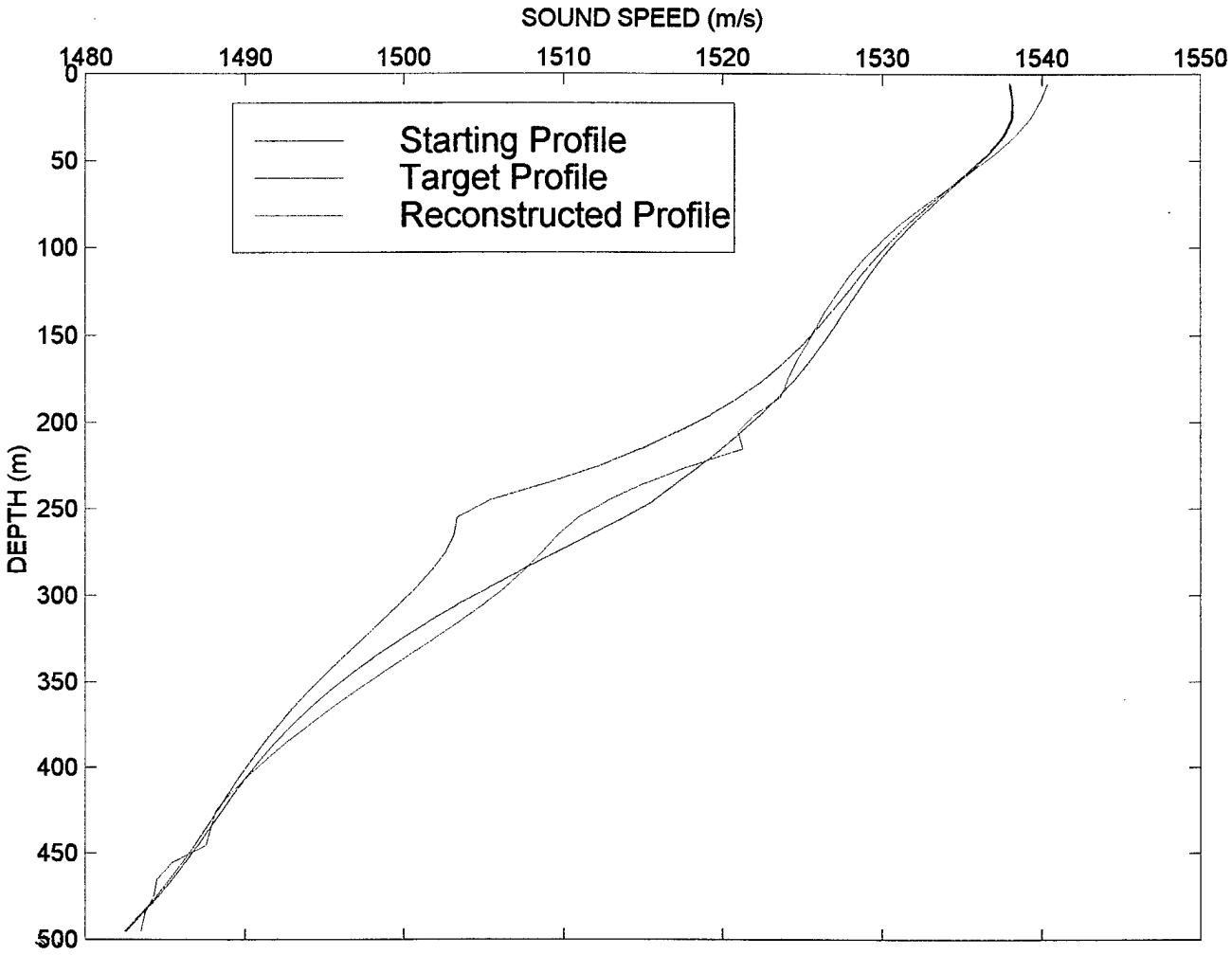

Figure 27. Starting, target, and reconstructed profiles.

Appendix A

	Rr	E-W (m)	N-S (m)	DEPTH (m)
1	1	7.9238856e+003	1.4035126e+004	1.6200120e+003
1	2	7.4529696e+003	1.1421161e+004	7.7784960e+002
1	3	7.5889104e+003	9.6002856e+003	6.8153280e+002
1	4	7.6029312e+003	7.4596752e+003	6.3581280e+002
1	5	6.8534280e+003	5.4827424e+003	6.3489840e+002
1	6	6.6422016e+003	3.9678864e+003	6.3825120e+002
1	7	6.3983616e+003	2.1110448e+003	6.3764160e+002
1	8	5.8792872e+003	-3.0937200e+002	6.4343280e+002
1	9	5.6580024e+003	-2.1872448e+003	6.4282320e+002
1	10	5.3309520e+003	-4.2635424e+003	6.4709040e+002
1	11	4.2976800e+003	-6.3959232e+003	6.9768720e+002
2	1	5.0285904e+003	1.2664135e+004	1.4813280e+003
2	2	5.0188368e+003	9.9020376e+003	7.5255120e+002
2	3	6.0844176e+003	8.0695800e+003	6.8823840e+002
2	4	5.1745896e+003	5.7902856e+003	6.8945760e+002
2	5	4.5963840e+003	3.6725352e+003	7.2603360e+002
2	6	4.2796968e+003	1.5252192e+003	7.1536560e+002
2	7	4.1535096e+003	-9.1135200e+002	7.5072240e+002
2	8	3.6603432e+003	-3.0370272e+003	7.6565760e+002
2	9	3.0571440e+003	-5.1797712e+003	7.5773280e+002
3	1	3.3680400e+003	7.9424784e+003	7.6931520e+002
3	2	2.4435816e+003	5.7293256e+003	7.7327760e+002
3	3	2.6828496e+003	3.0992064e+003	8.0619600e+002
3	4	2.2338792e+003	7.2146160e+002	8.3454240e+002
3	5	1.7763744e+003	-1.6099536e+003	8.5770720e+002
3	6	1.4773656e+003	-3.9416736e+003	8.2082640e+002
3	7	1.1350752e+003	-6.4492632e+003	8.2539840e+002
4	1	1.6011144e+003	1.2941808e+004	1.5660624e+003
4	2	2.3061168e+003	1.0731094e+004	1.3036296e+003
4	3	7.7480160e+002	7.9458312e+003	1.2390120e+003
4	4	2.8956000e+002	5.3413152e+003	1.3688568e+003
4	5	7.9248000e+000	2.9928312e+003	1.5215616e+003
4	6	-9.3329760e+002	5.4406800e+002	1.5767304e+003
4	7	-1.0399776e+003	-2.1582888e+003	1.5258288e+003
4	8	-1.5279624e+003	-4.6753272e+003	1.5203424e+003
4	9	-1.8266664e+003	-7.3362312e+003	1.4478000e+003
5	1	-1.0143744e+003	1.0658551e+004	1.5340584e+003
5	2	-2.2628352e+003	7.4977752e+003	1.6916400e+003
5	3	-2.7188160e+003	3.7112448e+003	1.7407128e+003
5	4	-3.6569904e+003	2.2860000e+002	1.7751552e+003
5	5	-3.9550848e+003	-3.0574488e+003	1.7623536e+003
5	6	-4.5884592e+003	-5.8283856e+003	1.6571976e+003

Table 1. Location of receivers in BARSTUR range.

Source	E-W (m)	N-S (m)	DEPTH (m)
UQC1	-2.9611e+003	-4.2425e+003	1.7297e+003
UQC2	-1.3219e+003	5.2044e+003	1.6434e+003
UQC3	3.0172e+003	2.0726e+004	3.0720e+003

Table 2. Location of sources in BARSTUR.